

# Microscopic theory of atom-molecule oscillations in a Bose-Einstein condensate

Thorsten Köhler, Thomas Gasenzer, and Keith Burnett

*Clarendon Laboratory, Department of Physics, University of Oxford, Oxford OX1 3PU, United Kingdom  
(October 27, 2018)*

In a recent experiment at JILA [E.A. Donley et al., *Nature (London)* **417**, 529 (2002)] an initially pure condensate of  $^{85}\text{Rb}$  atoms was exposed to a specially designed time dependent magnetic field pulse in the vicinity of a Feshbach resonance. The production of new components of the gas as well as their oscillatory behavior have been reported. We apply a microscopic theory of the gas to identify these components and determine their physical properties. Our time dependent studies allow us to explain the observed dynamic evolution of all fractions, and to identify the physical relevance of the pulse shape. Based on ab initio predictions, our theory strongly supports the view that the experiments have produced a molecular condensate.

PACS numbers: 03.75.Fi, 34.50.-s, 21.45.+v, 05.30.-d

## I. INTRODUCTION

The subject of the coupling between atoms and molecules in Bose-Einstein condensates has attracted intense interest following recent experiments [1–4]. Particular experiments we shall focus on are those performed at JILA [3,4] where the strength of the inter-atomic potential of  $^{85}\text{Rb}$  was varied rapidly using specially designed magnetic field pulses. This resulted in the loss of condensate atoms and the production of new components in the gas. One of these components is believed to be composed of molecules, and to be a molecular condensate. This is a remarkable achievement, with profound consequences for future work in the field. We shall show that this interpretation is fully supported by the theoretical work described in this article. We want to emphasize that the prediction of a molecular condensate arises naturally from the theory and does not have to be assumed at the outset. To make this prediction we use the microscopic theory of evolving condensed systems developed in Ref. [5]. This theory allows us to include the full dynamics of colliding pairs of atoms without the need for any assumptions about the nature of the states produced in the experiment. This theory gives us a generalization of the well known Gross-Pitaevskii equation (GPE) which includes the binary dynamics fully in the description of time evolving condensates.

If the variation in the magnetic field occurs slowly in comparison with the duration of a collision one should expect to be able to use the standard Gross-Pitaevskii approach [6] to the problem. The derivation of the GPE, however, relies precisely on the assumption that collisions occur on a timescale small compared to all others in the problem [5]. This approximation, therefore, fails in this new experimental regime where the magnetic field, tuned in the region of a Feshbach resonance, varies on this timescale.

As mentioned above the interpretation of the results of the experiment posits the production of bound molecular states, persisting at the end of the magnetic pulse sequence. Some theoretical treatments of the problem of molecules in condensates [7,8] separate out such states

as a separate entity of the physical system at the outset of their calculation, i.e. physical observables associated with two-body bound states are described in terms of a molecular quantum field that emerges directly in a model Hamiltonian [9].

In this article we give a microscopic treatment of the evolution of a Bose-Einstein condensate in the presence of a time varying magnetic field that completely avoids assumptions on the nature of the states involved in the collision process. In fact we treat the binary events involving bound and free molecular states formed during the evolution in a unified manner. This is a most sensible approach as strictly speaking, in the presence of the non-adiabatically time varying field there is no proper distinction between bound and free states. At the end of the pulse sequence we can of course resolve the final state of the gas into free and bound components. To do this we only use the assumption that the gas remains dilute and that binary encounters are the dominant collisional process. The evolution of pairs of particles from the condensate into other free states or into bound molecular states comes from this treatment. Our theory strongly supports the view that the experiments have produced a molecular condensate. We should emphasize again that this conclusion comes from an ab initio prediction of the theory and not as an assumption.

In the following sections we review briefly the microscopic theory of a dilute gas that we use in the analysis of the problem. We then show how the macroscopic evolution of the condensates is coupled in and out of the binary dynamics. We can then produce explicit expressions for the various components that are produced in the experiments. We have performed calculations, both for the case of the homogeneous gas and also for the case of a trapped condensate. The qualitative results of these two calculations agree but there are quantitative differences that merit further study. Our results for the loss of condensate and the production of a heated component agree with those produced in the experiment. In addition we are able to confirm the presence of a molecular condensate with all the physical properties we would expect.

## II. MICROSCOPIC DYNAMICS APPROACH

### A. Atomic mean field

The microscopic dynamics approach [5] is based on the general many body Hamiltonian for identical bosons with a pair interaction  $V(\mathbf{r}, t)$ ,

$$H = \int d^3x \psi^\dagger(\mathbf{x}) H_{1B}(\mathbf{x}) \psi(\mathbf{x}) + \frac{1}{2} \int d^3x d^3y \psi^\dagger(\mathbf{x}) \psi^\dagger(\mathbf{y}) V(\mathbf{x} - \mathbf{y}, t) \psi(\mathbf{y}) \psi(\mathbf{x}). \quad (1)$$

Here,  $H_{1B}(\mathbf{x}) = -\hbar^2 \nabla^2 / 2m + V_{\text{trap}}$  is the Hamiltonian of a single atom containing the kinetic energy and the trapping potential. The field operators satisfy bosonic commutation relations,  $[\psi(\mathbf{x}_1), \psi(\mathbf{x}_2)] = 0$ , and  $[\psi(\mathbf{x}_1), \psi^\dagger(\mathbf{x}_2)] = \delta(\mathbf{x}_1 - \mathbf{x}_2)$ . In the situation studied in this article, the inter-atomic interaction is varied using an external magnetic field pulse in the vicinity of a Feshbach resonance [4] and its time dependence is noted explicitly in Eq. (1).

All physical properties of a gas of atoms can be determined from correlation functions,  $\langle \psi^\dagger(\mathbf{x}_n) \cdots \psi(\mathbf{x}_1) \rangle_t$ , i.e. expectation values of normal ordered products of field operators with respect to the quantum state of the gas at time  $t$ . References [10,5] provide a general scheme to transform the exact infinite hierarchy of coupled dynamic equations for correlation functions into a more favorable form: The resulting equivalent set of dynamic equations for what are called non-commutative cumulants allows for a systematic truncation in accordance with Wick's theorem in statistical mechanics. In this article we apply this truncation scheme to determine a closed set of equations of motion for the relevant physical quantities. The derivation of the approach to the level of approximation required to study the phenomena reported in [4], i.e. the first order microscopic dynamics approach [5], is given in Appendix A.

The relevant physical quantities involve only the first and second order cumulants:

$$\begin{aligned} \Psi(\mathbf{x}, t) &= \langle \psi(\mathbf{x}) \rangle_t, \\ \Phi(\mathbf{x}, \mathbf{y}, t) &= \langle \psi(\mathbf{y}) \psi(\mathbf{x}) \rangle_t - \langle \psi(\mathbf{y}) \rangle_t \langle \psi(\mathbf{x}) \rangle_t, \\ \Gamma(\mathbf{x}, \mathbf{y}, t) &= \langle \psi^\dagger(\mathbf{y}) \psi(\mathbf{x}) \rangle_t - \langle \psi^\dagger(\mathbf{y}) \rangle_t \langle \psi(\mathbf{x}) \rangle_t. \end{aligned} \quad (2)$$

Here,  $\Psi(\mathbf{x}, t)$  is the atomic mean field,  $\Phi(\mathbf{x}, \mathbf{y}, t)$  the pair function, which plays an important role in the description of correlated pairs of atoms, and  $\Gamma(\mathbf{x}, \mathbf{y}, t)$  is the one-body density matrix of the non-condensed fraction. The density of the gas at the position  $\mathbf{x}$  and time  $t$  is thus given by  $n(\mathbf{x}, t) = \langle \psi^\dagger(\mathbf{x}) \psi(\mathbf{x}) \rangle_t = \Gamma(\mathbf{x}, \mathbf{x}, t) + |\Psi(\mathbf{x}, t)|^2$ .

In the first order microscopic dynamics approach the atomic mean field is determined through a closed nonlinear Schrödinger equation [5]:

$$\begin{aligned} i\hbar \frac{\partial}{\partial t} \Psi(\mathbf{x}, t) &= H_{1B}(\mathbf{x}) \Psi(\mathbf{x}, t) \\ &- \Psi^*(\mathbf{x}, t) \int_{t_0}^{\infty} d\tau \Psi^2(\mathbf{x}, \tau) \frac{\partial}{\partial \tau} h(t, \tau). \end{aligned} \quad (3)$$

The collision term distinguishes the non-Markovian dynamic Eq. (3) from the Gross-Pitaevskii approach and is determined through the coupling function

$$h(t, \tau) = (2\pi\hbar)^3 \langle 0 | V(t) U_{2B}(t, \tau) | 0 \rangle \theta(t - \tau), \quad (4)$$

where  $U_{2B}(t, \tau)$  denotes the unitary time development operator of the relative motion of two atoms in free space,  $|0\rangle$  is the zero momentum plane wave and  $\theta(t - \tau)$  is the step function which gives unity for  $t > \tau$  and vanishes elsewhere. Throughout this article the three dimensional plane wave with momentum  $\mathbf{p}$  is normalized as  $\langle \mathbf{r} | \mathbf{p} \rangle = \exp(i\mathbf{p} \cdot \mathbf{r} / \hbar) / \sqrt{2\pi\hbar^3}$ .

### B. Non-condensed fraction

In the first order microscopic dynamics approach the nonlinear Schrödinger Eq. (3) determines not only the atomic mean field but also the pair function,  $\Phi$ , and, in turn, the density matrix of the non-condensed fraction,  $\Gamma$ , in Eq. (2). The pair function is given by

$$\begin{aligned} \Phi(\mathbf{x}, \mathbf{y}, t) &= - \int_{t_0}^t d\tau \int d^3x' d^3y' \Psi(\mathbf{x}', \tau) \Psi(\mathbf{y}', \tau) \\ &\times \frac{\partial}{\partial \tau} \langle \mathbf{x}, \mathbf{y} | U_{\text{trap}}^{2B}(t, \tau) | \mathbf{x}', \mathbf{y}' \rangle, \end{aligned} \quad (5)$$

where  $U_{\text{trap}}^{2B}(t, \tau)$  is the unitary time development operator of two trapped atoms interacting through the pair potential  $V(t)$ . The density matrix of the non-condensed fraction expressed in terms of the pair function is given by

$$\Gamma(\mathbf{x}, \mathbf{y}, t) = \int d^3x' \Phi(\mathbf{x}, \mathbf{x}', t) \Phi^*(\mathbf{y}, \mathbf{x}', t). \quad (6)$$

As shown in Appendix A, Eq. (6) assures both the positivity of all occupation numbers and the conservation of the total number of atoms in the gas:

$$\int d^3x [|\Psi(\mathbf{x}, t)|^2 + \Gamma(\mathbf{x}, \mathbf{x}, t)] = N_c(t) + N_{nc}(t) = N. \quad (7)$$

The form of Eq. (6) suggests a separation of the number of non-condensed atoms into a molecular fraction and correlated pairs of atoms after a time dependent magnetic field pulse of the kind reported in Ref. [4] as follows: The total number of non-condensed atoms is given by

$$\begin{aligned} N_{nc}(t) &= \int d^3x \Gamma(\mathbf{x}, \mathbf{x}, t) = \int d^3x d^3x' |\Phi(\mathbf{x}, \mathbf{x}', t)|^2 \\ &= \int d^3R d^3r |\Phi(\mathbf{R}, \mathbf{r}, t)|^2, \end{aligned} \quad (8)$$

where the position dependence was changed to two body center of mass and relative coordinates  $\mathbf{R} = (\mathbf{x} + \mathbf{y})/2$

and  $\mathbf{r} = \mathbf{y} - \mathbf{x}$ , respectively. Under the assumption that the trap is switched off at time  $t_{\text{fin}}$ , immediately after the pulse, and the magnetic field is held constant at its final value, the energy states of the relative motion of a pair of atoms become stationary. A complete set of energy eigenstates is given through

$$1 = \sum_{\nu} |\phi_{b\nu}\rangle\langle\phi_{b\nu}| + \int d^3p |\phi_{\mathbf{p}}^{(+)}\rangle\langle\phi_{\mathbf{p}}^{(+)}|, \quad (9)$$

where  $\phi_{b\nu}$  are the molecular bound states of the final pair potential and  $\phi_{\mathbf{p}}^{(+)}$  are chosen as stationary scattering states which, at large relative distance, become a sum of an incoming plane wave with momentum  $\mathbf{p}$  and an outgoing spherical wave (see, e.g., [11] or Appendix B). Replacing the spatial integration over the relative coordinate  $\mathbf{r}$  in Eq. (8) in favor of the energy eigenstates in Eq. (9) the non-condensed fraction splits into a molecular part and a scattering part:

$$N_{\text{nc}}(t) = \int d^3R \left[ \sum_{\nu} |\langle\mathbf{R}, \phi_{b\nu}|\Phi(t)\rangle|^2 + \int d^3p |\langle\mathbf{R}, \phi_{\mathbf{p}}^{(+)}|\Phi(t)\rangle|^2 \right], \quad (10)$$

where  $|\Phi(t)\rangle \equiv \int d^3R d^3r |\mathbf{R}, \mathbf{r}\rangle\Phi(\mathbf{R}, \mathbf{r}, t)$ . The choice of eigenstates and the physical meaning of the contributions to Eq. (10) depend on the experimental situation to be described. As will be shown in the next subsections the molecular part in Eq. (10) determines the number of atoms bound to molecules after the pulse while the scattering part describes pairs of atoms emitted from the condensate in a ballistic expansion.

### C. Molecular fraction

The operator that determines the number of pairs of atoms in the specific bound state  $\phi_b$  in a gas with  $N$  atoms reads, in its first quantization form,

$$\mathcal{N}_b = \frac{1}{2} \sum_{\substack{i,j=1 \\ i \neq j}}^N |\phi_{b,ij}\rangle\langle\phi_{b,ij}|, \quad (11)$$

where  $i$  and  $j$  indicate the pair of atoms. Expressed in terms of the atomic field operator Eq. (11) becomes:

$$\begin{aligned} \mathcal{N}_b &= \frac{1}{2} \int d^3x_1 d^3x_2 d^3x'_1 d^3x'_2 \phi_b(\mathbf{x}'_2 - \mathbf{x}'_1) \phi_b^*(\mathbf{x}_2 - \mathbf{x}_1) \\ &\quad \times \delta\left(\frac{1}{2}(\mathbf{x}'_1 + \mathbf{x}'_2) - \frac{1}{2}(\mathbf{x}_1 + \mathbf{x}_2)\right) \\ &\quad \times \psi^\dagger(\mathbf{x}'_1) \psi^\dagger(\mathbf{x}'_2) \psi(\mathbf{x}_2) \psi(\mathbf{x}_1). \end{aligned} \quad (12)$$

The mean number of molecules in the state  $|\phi_b\rangle$  is thus given by

$$\begin{aligned} N_b(t) &= \langle\mathcal{N}_b\rangle_t = \frac{1}{2} \int d^3r' d^3r d^3R \phi_b(\mathbf{r}') \phi_b^*(\mathbf{r}) \\ &\quad \times \left\langle \psi^\dagger\left(\mathbf{R} + \frac{\mathbf{r}'}{2}\right) \psi^\dagger\left(\mathbf{R} - \frac{\mathbf{r}'}{2}\right) \psi\left(\mathbf{R} - \frac{\mathbf{r}}{2}\right) \psi\left(\mathbf{R} + \frac{\mathbf{r}}{2}\right) \right\rangle_t, \end{aligned} \quad (13)$$

where  $\mathbf{R}$  and  $\mathbf{r}$  are center of mass and relative coordinates, respectively. The fourth order correlation function in Eq. (13) can be factorized into cumulants (cf. Eq. (A4)), and truncated in accordance with the level of approximation of the first order microscopic dynamics approach:

$$\begin{aligned} &\langle \psi^\dagger(\mathbf{x}_4) \psi^\dagger(\mathbf{x}_3) \psi(\mathbf{x}_2) \psi(\mathbf{x}_1) \rangle_t \\ &= \langle \psi^\dagger(\mathbf{x}_4) \psi^\dagger(\mathbf{x}_3) \rangle_t \langle \psi(\mathbf{x}_2) \psi(\mathbf{x}_1) \rangle_t. \end{aligned} \quad (14)$$

The mean number of molecules in the state  $|\phi_b\rangle$  can then be expressed in terms of a molecular mean field as

$$N_b(t) = \int d^3R |\Psi_b(\mathbf{R}, t)|^2, \quad (15)$$

where

$$\begin{aligned} \Psi_b(\mathbf{R}, t) &= \frac{1}{\sqrt{2}} \int d^3r \phi_b^*(\mathbf{r}) \\ &\quad \times [\Phi(\mathbf{R}, \mathbf{r}, t) + \Psi(\mathbf{R} + \frac{\mathbf{r}}{2}, t) \Psi(\mathbf{R} - \frac{\mathbf{r}}{2}, t)]. \end{aligned} \quad (16)$$

The overlap of the molecular wave function  $\phi_b$  with the second, factorized term on the right hand side of Eq. (16) can be shown to be negligible in all applications described in this article. The molecular part on the right hand side of Eq. (10) is thus twice the number of dimer molecules in the gas, i.e. the number of atoms bound to dimer molecules. The wave function  $\Psi_b(\mathbf{R}, t)$ , which yields the density of the molecular fraction, is thus obtained systematically in terms of atomic field correlation functions. The derivation leading to Eqs. (15) and (16) does not depend on  $\phi_b$  being a bound state. The number of pairs of atoms in any two body state is obtained in an analogous way. In Subsection IID we will apply an analogue of Eqs. (15) and (16) to determine the number of atoms emitted from the condensate during the magnetic field pulse.

### D. Burst of atoms

In this subsection we show that the scattering part of the non condensed fraction on the right hand side of Eq. (10) determines the number of relatively hot atoms emitted in pairs from the condensate. To this end we consider a ballistic expansion of the gas at time  $t_{\text{fin}}$ , i.e. the trap is switched off and the magnetic field is held constant immediately at the end of a magnetic field pulse. This is illustrated schematically in Fig. 1.

A relatively hot fraction, if present, will expand much faster than the condensate and can be detected far outside the remnant condensate at a time  $t$  sufficiently long after  $t_{\text{fin}}$ . For a gas with  $N$  atoms the observable for the number of pairs of atoms with a relative coordinate between  $\mathbf{r}$  and  $\mathbf{r} + d^3r$ , in its first quantization form, is given by  $\sum_{i < j} |\mathbf{r}_{ij}\rangle\langle\mathbf{r}_{ij}| d^3r$ , where, as in Subsection II C,

$i$  and  $j$  indicate the pair of atoms. In complete analogy to Subsection II C the mean number of pairs of atoms with a relative coordinate between  $\mathbf{r}$  and  $\mathbf{r} + d^3r$  becomes

$$n_{\mathbf{r}}(t)d^3r = \int d^3R |\Psi_{\mathbf{r}}(\mathbf{R}, t)|^2 d^3r, \quad (17)$$

where

$$\Psi_{\mathbf{r}}(\mathbf{R}, t) = \frac{1}{\sqrt{2}} [\Phi(\mathbf{R}, \mathbf{r}, t) + \Psi(\mathbf{R} + \frac{\mathbf{r}}{2}, t)\Psi(\mathbf{R} - \frac{\mathbf{r}}{2}, t)]. \quad (18)$$

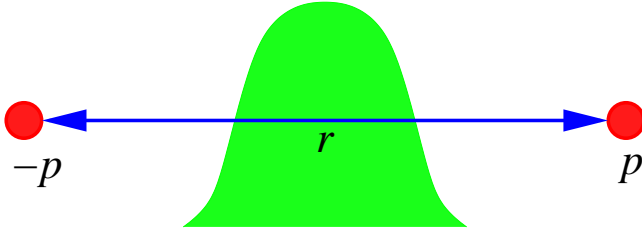


FIG. 1. Scheme of a ballistic expansion after a magnetic field pulse. Pairs of atoms are emitted from the condensate with one-particle momenta  $\mathbf{p}$  and  $-\mathbf{p}$ . The center of mass of the pairs stays confined in the remnant condensate with a momentum spread determined by the spread of momenta in the condensate. At a sufficiently long time after the pulse a burst of relatively hot atoms can be detected outside the remnant condensate.

At the relative distances  $r$  under consideration, which exceed by far the size of the remnant condensate, the second, factorized contribution to Eq. (18) is negligible. The energy spectrum of the relatively hot atoms can be obtained from an expansion of  $\Psi_{\mathbf{r}}$  in terms of the energy states in Eq. (9) that correspond to a release of the atoms from the trap:

$$\Psi_{\mathbf{r}}(\mathbf{R}, t) = \frac{1}{\sqrt{2}} \sum_{\nu} \phi_{b\nu}(\mathbf{r}) \langle \mathbf{R}, \phi_{b\nu} | \Phi(t) \rangle + \frac{1}{\sqrt{2}} \int d^3p \phi_{\mathbf{p}}^{(+)}(\mathbf{r}) \langle \mathbf{R}, \phi_{\mathbf{p}}^{(+)} | \Phi(t) \rangle. \quad (19)$$

The molecular wave functions in Eq. (19) have decayed at the relevant distances  $r$  that even exceed the extent of the remnant condensate. The corresponding molecular contribution to the right hand side of Eq. (19) is thus negligible. Taking into account that the scattering wave functions  $\phi_{\mathbf{p}}^{(+)}$  are energy eigenstates of a pair of atoms after the pulse the remaining part of the amplitude in Eq. (19) becomes, after a short calculation using Eq. (5),

$$\Psi_{\mathbf{r}}(\mathbf{R}, t) = \frac{1}{\sqrt{2}} \int d^3p \phi_{\mathbf{p}}^{(+)}(\mathbf{r}) \langle \mathbf{R}, \phi_{\mathbf{p}}^{(+)} | \Phi(t_{\text{fin}}) \rangle \times e^{-i\frac{\mathbf{p}^2}{m}(t-t_{\text{fin}})/\hbar}. \quad (20)$$

For two identical atoms the relative kinetic energy  $E_{\text{rel}}$  and the relative momentum  $\mathbf{p}$  are related through  $E_{\text{rel}} =$

$\mathbf{p}^2/m$ . The spectrum of the pairs of comparatively hot atoms, i.e. the number of pairs of atoms with a relative energy in the interval  $E_{\text{rel}} \dots E_{\text{rel}} + dE_{\text{rel}}$ , is thus given by:

$$n(E_{\text{rel}})dE_{\text{rel}} = \frac{1}{2} \sqrt{m^3} \sqrt{E_{\text{rel}}} dE_{\text{rel}} \times \int d\Omega_{\mathbf{p}} \int d^3R |\Psi_{\mathbf{p}}(\mathbf{R})|^2, \quad (21)$$

where  $\Psi_{\mathbf{p}}(\mathbf{R}) = \langle \mathbf{R}, \phi_{\mathbf{p}}^{(+)} | \Phi(t_{\text{fin}}) \rangle / \sqrt{2}$  is the amplitude on the right hand side of Eq. (20) and  $d\Omega_{\mathbf{p}}$  denotes the angular component of  $d^3p$ . The sum over all energy components of the spectrum yields

$$\int_0^{\infty} n(E_{\text{rel}})dE_{\text{rel}} = \frac{1}{2} \int d^3p \int d^3R |\langle \mathbf{R}, \phi_{\mathbf{p}}^{(+)} | \Phi(t_{\text{fin}}) \rangle|^2. \quad (22)$$

A comparison between Eqs. (10), (15) and (22) shows that the total non-condensed fraction of the gas consists of molecules and a burst of comparatively hot atoms emitted in pairs from the condensate with a time of flight spectrum of relative energies given by Eq. (21). Whether the non condensed fraction becomes significant depends on the time dependence of the magnetic field, i.e. the way energy is released to the gas.

### III. DYNAMICS OF THE GAS

#### A. Feshbach resonance and magnetic field pulse

In this Section we discuss the evolution of the gas when a specially designed homogeneous magnetic field pulse is applied to tune the inter-atomic interaction rapidly in the vicinity of a Feshbach resonance. Motivated by the experiment of Donley et al. [4] we study the time variation of the magnetic field shown in Fig. 2. The magnetic field varies linearly in time within the subsequent time intervals.

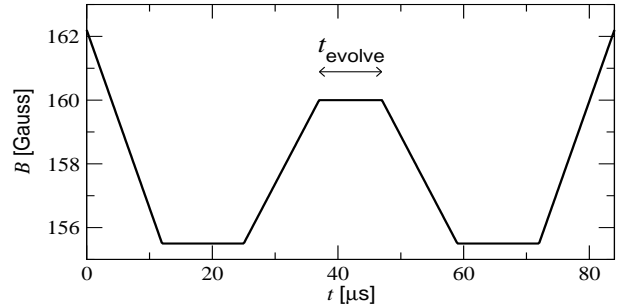


FIG. 2. Time dependence of the magnetic field. The field varies linearly within the subsequent time intervals. The numerical simulations in this article have been performed with the following pulse shape: Fall and rise times:  $12 \mu\text{s}$ ; hold time at  $B = 155.5 \text{ G}$ :  $13 \mu\text{s}$ ; evolution time at  $B = 160 \text{ G}$ :  $t_{\text{evolve}} = 10 \dots 40 \mu\text{s}$ ; initial and final fields:  $B = 162.2 \text{ G}$ .

A Feshbach resonance occurs when the energy of a bound state of a closed channel potential is tuned close to the dissociation threshold of the ground state potential [12]. This tuning of the interaction in the inter-atomic motion takes advantage of the Zeeman effect in the electronic energy levels of the atoms. If the closed channel bound state approaches the threshold from below, the inter-atomic potential supports a shallow (metastable)  $s$  wave bound state. Around the resonance, a slight change in the energy difference of the potentials thus leads to a large variation of the scattering length. Neglecting the slow decay of the  $s$  wave bound state, the scattering length depends on the magnetic field through the relation

$$a(B) = a_{\text{bg}} \left( 1 - \frac{\Delta B}{B - B_0} \right), \quad (23)$$

where  $\Delta B$  is the width of the Feshbach resonance and  $B_0$  is the resonant field. We consider the resonance of  $^{85}\text{Rb}$  at  $B_0 = 154.9$  G, with  $\Delta B = 11.0$  G [13], which has been used in [4]. For the background scattering length we use the value  $a_{\text{bg}} = -450 a_{\text{Bohr}}$  [4], where  $a_{\text{Bohr}}$  is the Bohr-radius.

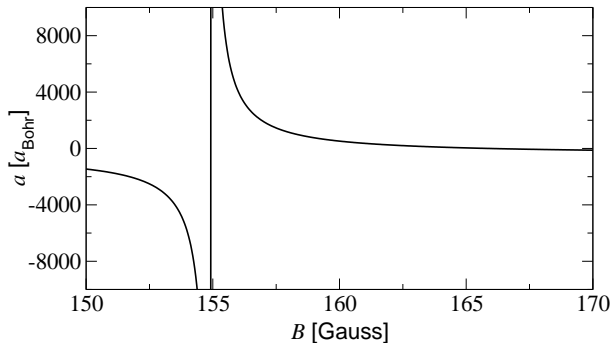


FIG. 3. The scattering length  $a$  in units of the Bohr radius, as a function of the magnetic field  $B$ , in the vicinity of the Feshbach resonance.  $a(B)$  is determined from Eq. (23), using  $B_0 = 154.9$  G,  $\Delta B = 11.0$  G, and  $a_{\text{bg}} = -450 a_{\text{Bohr}}$ .

Figure 3 shows the scattering length as a function of the field  $B$  in the vicinity of the resonance for the values of  $B$  that are relevant in this article. At the initial time  $t_0$ , the magnetic field  $B = 162.2$  G implies a scattering length of about  $228 a_{\text{Bohr}}$  (cf. Fig. 3). The interactions then vary according to the pulse shape in Fig. 2. Similar to the experimental procedure [4] we will determine the dynamic evolution of the gas for fixed time constants and field strengths of the initial and final pulses, but for different evolution times  $t_{\text{evolve}}$ .

In the experiment [4] an adiabatic field variation followed the pulse sequence. Finally the trap and the magnetic field were switched off, and the gas freely expanded before the number of atoms in the remnant condensate as well as a burst of relatively hot atoms were detected by absorption imaging. A series of measurements was

performed for varying evolution times  $t_{\text{evolve}}$ . The number of atoms in each component showed an oscillatory dependence on  $t_{\text{evolve}}$  with the frequency corresponding to the energy of the shallow two body  $s$  wave bound state in the evolution period. Moreover, a fraction of missing atoms was found oscillating at the same frequency. An interesting side result reported in [4] is that the visibility of the oscillations depended sensitively on the presence of the initial and final ramp very close to the resonance (at 155.5 G in Fig. 2). In the next subsections we shall explain these observations.

## B. Coupling function

We will study first the coupling function of the non-Markovian non-linear Schrödinger Eq. (3) for magnetic field variations as shown in Fig. 2. The coupling function  $h(t, \tau)$ , given in Eq. (4), reflects the binary dynamics that enters the description of the condensate through Eq. (3). We will discuss to which extent the binary dynamics can already explain why the particular field pulse was needed to observe the oscillations between the condensate and the non condensed fraction of the gas.

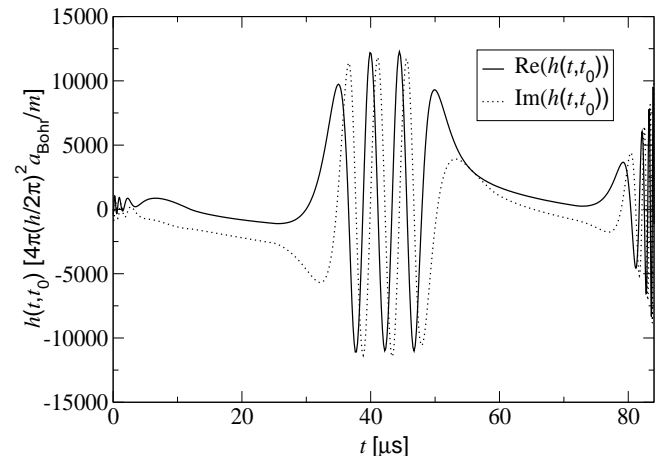


FIG. 4. The coupling function  $h(t, \tau)$  as a function of  $t$ , describing the two-body dynamics driven by the magnetic field pulse in Fig. 2, for  $\tau = t_0$ , and an evolution time  $t_{\text{evolve}} = 10 \mu\text{s}$ .

We have numerically determined the time dependence of  $h(t, \tau)$  in the two dimensional plane  $(t, \tau)$  for  $t_0 < t < t_{\text{fin}}$  and  $t_0 < \tau < t$  using the methods described in Appendix B. Figure 4 shows  $h(t, \tau)$  as a function of  $t$ , for  $\tau = t_0$  and the time dependence of the magnetic field in Fig. 2, with  $t_{\text{evolve}} = 10 \mu\text{s}$ . In the evolution period between  $t_3 = 37 \mu\text{s}$  and  $t_4 = 47 \mu\text{s}$ ,  $h(t, \tau)$  oscillates with the frequency  $\nu_{\text{evolve}} \cong 200$  kHz. This particular oscillatory dependence is to be expected, as, according to Eq. (4),  $h(t, \tau)$  involves the two body time development operator,  $U_{2\text{B}}(t, \tau)$ : In this period the binary potential is stationary and supports a shallow  $s$  wave bound state

$\phi_b^{\text{evolve}}$ . A spectral decomposition of  $U_{2B}(t, \tau)$  shows that the contribution of this bound state to  $h(t, \tau)$ , within the evolution period, is given by:

$$h(t, \tau) \cong (2\pi\hbar)^3 \langle 0|V(t)|\phi_b^{\text{evolve}}\rangle \langle \phi_b^{\text{evolve}}|U_{2B}(t_3, \tau)|0\rangle \times \theta(t - \tau) e^{-iE_b^{\text{evolve}}(t-t_3)/\hbar}, \quad (24)$$

where  $t_3$  is the initial time of the evolution period. The frequency of the oscillations in the coupling function thus corresponds to the bound state energy in the evolution period, i.e.  $\nu_{\text{evolve}} = |E_b^{\text{evolve}}|/\hbar$ . The amplitude and phase of these oscillations, however, depend on the time evolution before.

The particularly large amplitude in Fig. 4 is achieved by the initial ramp close to the resonance at  $B \cong 155$  G in Fig. 2. To illustrate the role of the first ramp, Fig. 5 shows  $h(t, \tau)$  as a function of  $t$ , at  $\tau = t_0$ , for a trapezoidal pulse. Here, the trapezoidal pulse is chosen similar to Fig. 2 except that the initial and final ramps to  $B = 155.5$  G are cut off, i.e. the magnetic field is held constant at 160 G between  $t \cong 4 \mu\text{s}$  and  $t \cong 80 \mu\text{s}$ . As shown in Figs. 4 and 5 the first ramp to  $B = 155.5$  G causes a pronounced enhancement of the amplitude by a factor of about 20 for the optimized pulse in Fig. 2 as compared to the trapezoidal pulse.

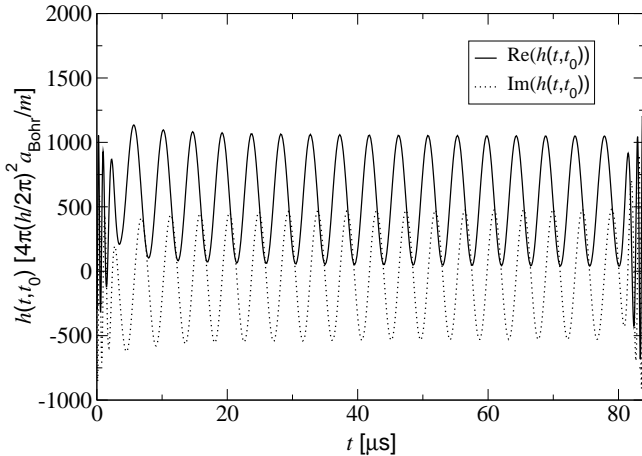


FIG. 5. The coupling function  $h(t, \tau)$  as a function of  $t$ , for  $\tau = t_0$ , describing the two-body dynamics for a trapezoidal pulse, i.e. the magnetic field pulse in Fig. 2 but without the initial and final ramps to  $B = 155.5$  G. The magnetic field is thus held constant at  $B = 160$  G from  $t \cong 4 \mu\text{s}$  to  $t \cong 80 \mu\text{s}$ .

Figure 6 shows the real and imaginary part of  $h(t, \tau)$  in the two-dimensional plane  $(t, \tau)$ , for the same parameters as in Fig. 4. The figure reveals that the amplitude of the oscillations during the evolution period between  $t = 37 \mu\text{s}$  and  $t = 47 \mu\text{s}$  rapidly decays in  $\tau$ . The phase of the oscillations, however, is largely independent of  $\tau$ . A further analysis shows that these properties of the especially optimized pulse form in Fig. 2 assure the reappearance

of the oscillation frequency of  $h(t, \tau)$  in the nonlinear dynamics of the condensate described by Eq. (3).

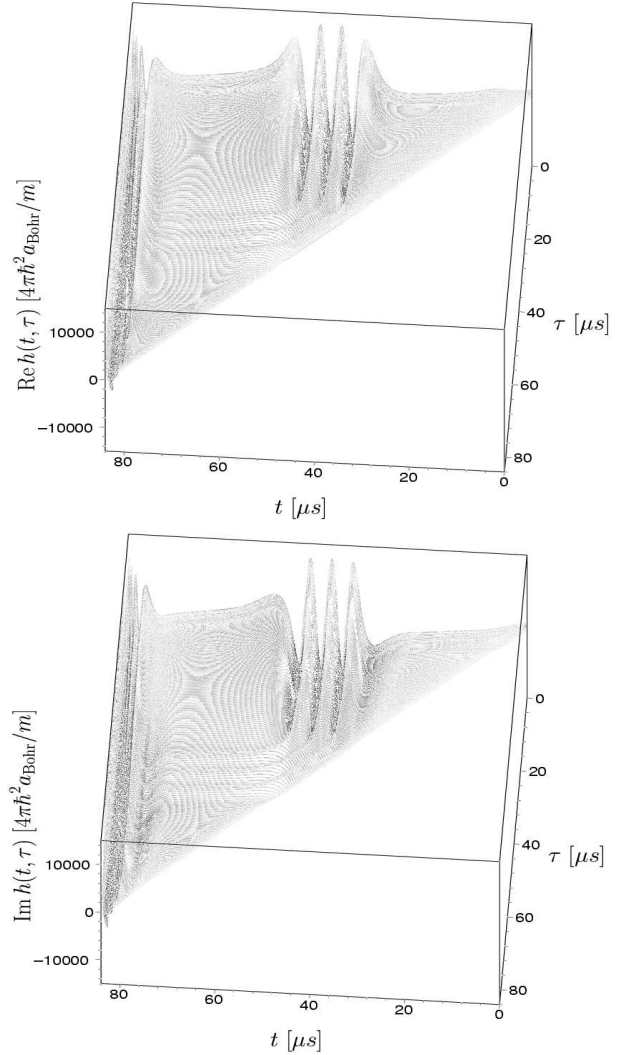


FIG. 6. The coupling function  $h(t, \tau)$  as a function of  $t$  and  $\tau$ , for the same parameters as used in Fig. 4.

### C. Homogeneous gas

The dynamics of a homogeneous condensate driven by a magnetic field pulse of the form in Fig. 2 already exhibits all basic qualitative phenomena reported in [4]. We will therefore study the time evolution of the condensate as well as the final non-condensed fraction in detail for this idealized gas. Thereafter, we will discuss the corrections due to the presence of a trap in Subsection III D. All physical quantities under consideration are determined by the nonlinear Schrödinger Eq. (3), driven by coupling functions of the form of Fig. 6, with a variable evolution time  $t_{\text{evolve}}$ .

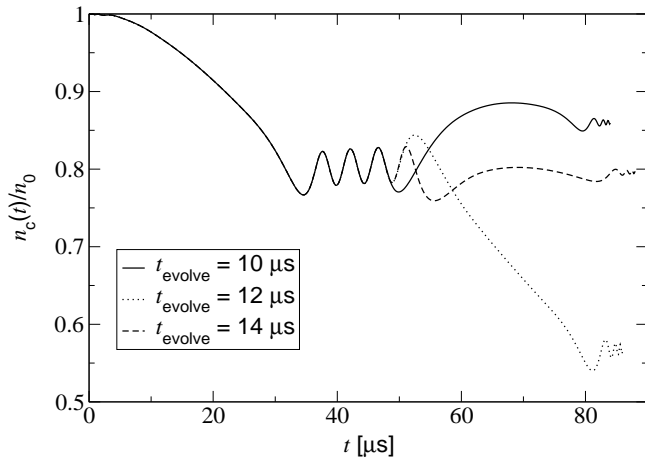


FIG. 7. The time dependence of the relative condensate fraction  $n_c(t)/n_0$  remaining of the initial density of  $n_0 = 3.9 \times 10^{12} \text{ cm}^{-3}$  for three different evolution times  $t_{\text{evolve}} = 10 \mu\text{s}$ ,  $12 \mu\text{s}$ , and  $14 \mu\text{s}$ . The sequence of magnetic field pulses is chosen as in Fig. 2 with a field strength in the evolution period of  $B_{\text{evolve}} = 160 \text{ G}$ .

Starting from a pure condensate with the density  $n_0 = 3 \times 10^{12} \text{ cm}^{-3}$ , Fig. 7 shows the relative atomic condensate density  $n_c(t)/n_0$ , as a function of  $t$ , for three different evolution times  $t_{\text{evolve}} = 10 \mu\text{s}$ ,  $12 \mu\text{s}$ , and  $14 \mu\text{s}$ . The initial conditions correspond roughly to the low density measurements in Ref. [4]. After an initial loss period during  $t_0 = 0 \leq t \lesssim 35 \mu\text{s}$  the condensate density shows a distinct oscillatory behavior around 80% of the initial density. The frequency of these oscillations very precisely matches the bound state frequency in the evolution period, i.e.  $\nu_{\text{evolve}} = |E_{\text{b}}^{\text{evolve}}|/h \cong 200 \text{ kHz}$ . After the evolution period, the second magnetic field pulse, which shifts the atoms in and out of the vicinity of the Feshbach resonance, causes the condensate fraction to develop to values between 55% and 85%. The final fraction depends on the phase of the intermediate oscillations at the end of the evolution period when the second resonant pulse starts. The remnant condensate density at time  $t_{\text{fin}}$ , immediately after the pulse sequence, therefore, also oscillates as a function of  $t_{\text{evolve}}$ . While the first ramp to  $B = 155.5 \text{ G}$  in Fig. 2 drives the amplitude of the oscillations of  $n_c(t)$  in  $t$  the second ramp in Fig. 2 amplifies the visibility of the oscillations in  $n_c(t_{\text{fin}})$  as a function of  $t_{\text{evolve}}$ . The fast oscillations of the function  $h(t, \tau)$  in  $t$  at the very beginning and ending of the pulse sequence (see Figs. 4 and 6) have only a minor influence on the evolution of the condensate.

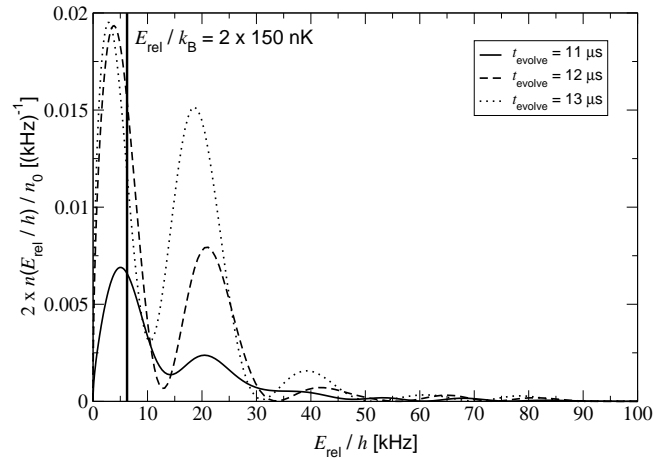


FIG. 8. The density of burst atoms ( $2 \times n(E_{\text{rel}})$  with  $n(E_{\text{rel}})$  given by Eq. (21)) as a function of the relative energy  $E_{\text{rel}}$  in a uniform gas for three different evolution times  $t_{\text{evolve}} = 11 \mu\text{s}$ ,  $12 \mu\text{s}$ , and  $13 \mu\text{s}$ . The external parameters are chosen as in Fig. 7. The atoms are emitted from the condensate in pairs with momenta  $\mathbf{p}$  and  $-\mathbf{p}$ . The relative energy  $E_{\text{rel}} = \mathbf{p}^2/m$  is related to the energy of a single atom,  $E_{1\text{B}} = \mathbf{p}^2/2m$ , through  $E_{1\text{B}} = E_{\text{rel}}/2$ . The vertical line indicates the scale of the mean energies of burst atoms reported in Ref. [4].

The atomic mean field  $\Psi$  determines the pair function through Eq. (5) and, in turn, the molecular fraction in Eqs. (15) and (16) as well as the energy spectrum of comparatively hot atoms, Eq. (21), after the pulse. Figure 8 shows the density of atoms emitted in pairs from the condensate as a function of their relative energy for a uniform gas under the conditions described in Fig. 7. As the momentum spread of the center of mass motion of the pairs corresponds to the small spread of momenta in the atomic condensate the energy of a single atom in a pair is related to the relative energy through  $E_{1\text{B}} = E_{\text{rel}}/2$ . The spectra exhibit a damped oscillatory dependence on the energy with a first, dominant maximum below  $E_{1\text{B}}/k_{\text{B}} = 150 \text{ nK}$ . The time of flight energy spectra in Fig. 8, as described in Subsection IID, do not correspond completely to the experimental procedure in [4]. The presence of a trap should also modify their shape in a noticeable way. We expect, however, that Fig. 8 reflects the typical energy scales of the burst atoms in Ref. [4].

The experimental procedure did not allow for a direct detection of molecules. We thus identify the fraction of missing atoms reported in [4] as those atoms that are bound to dimer molecules after the pulse sequence. The total density of unbound atoms is then given by the initial density  $n_0$  minus twice the density of dimer molecules in the homogeneous gas. In the course of our studies we have determined the remnant condensate as well as the final molecular fraction as a function of the evolution time  $t_{\text{evolve}}$  from 10 to  $40 \mu\text{s}$  in steps of  $1 \mu\text{s}$ . The total length of the pulses has thus been varied between  $84 \mu\text{s}$  and  $114 \mu\text{s}$ .

The results are summarized in Fig. 9. The solid line is an interpolation of the data for the remnant condensate

density relative to the initial density of  $n_0 = 3.9 \times 10^{12} \text{ cm}^{-3}$  (filled circles) with the sinusoidal fit function proposed by Donley et al. [4]. The frequency of the oscillations corresponds to the binding energy  $|E_b^{\text{evolve}}|/h = |E_b(160 \text{ G})|/h \cong 200 \text{ kHz}$ . In Fig. 9 the filled squares and their interpolation, i.e. the uppermost curve, show the fraction of atoms which are not bound to dimer molecules after the magnetic field pulse (Fig. 2). Number conservation allows to determine the density of the burst of relatively hot atoms directly from the total density of unbound atoms and the remnant condensate (cf. Eqs. (7) and (10)). For this reason the dotted curve in Fig. 9, termed “burst of atoms”, has been obtained by subtracting the solid curve from the dashed curve. Both the fraction of “missing” atoms and the “burst” of atoms exhibit oscillations with the frequency  $\nu_{\text{evolve}} = |E_b^{\text{evolve}}|/h$  in  $t_{\text{evolve}}$  as well as the phase relation with respect to the remnant condensate reported in [4].

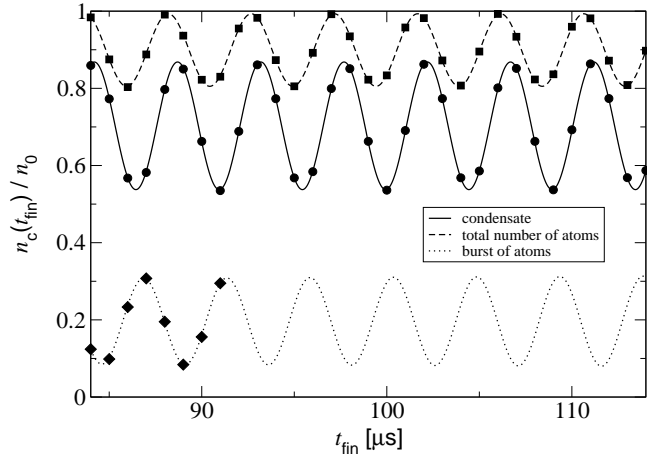


FIG. 9. The remaining fraction of condensate atoms,  $n_c(t_{\text{fin}})$ , (solid line) together with the total density of unbound atoms (dashed line) in a homogeneous gas, as a function of the final time  $t_{\text{fin}}$ , elapsed after a magnetic field pulse of the form in Fig. 2. All densities are given relative to the initial density of  $n_0 = 3.9 \times 10^{12} \text{ cm}^{-3}$ . The external parameters are chosen as in Fig. 2. The filled circles and squares correspond to direct calculations of the remnant condensate and the molecular fraction. The solid and dashed curves are interpolations with the sinusoidal fit functions proposed in Ref. [4]. The dotted line indicates the “burst” of relatively hot (unbound) atoms emitted in pairs from the condensate as determined from the remnant condensate and the total fraction of unbound atoms through number conservation (cf. Eqs. (7) and (10)). The filled diamonds correspond to direct calculations of the “burst” fraction obtained from integration of the spectra in Fig. 8 with respect to the energy.

#### D. Trapped gas

The studies of the homogeneous gas in Subsection III C allowed to identify the three components of the gas as observed in [4]. The purpose of this subsection is to

study the influence of the trap and the inhomogeneous local densities of the gas on the relative magnitudes of these components.

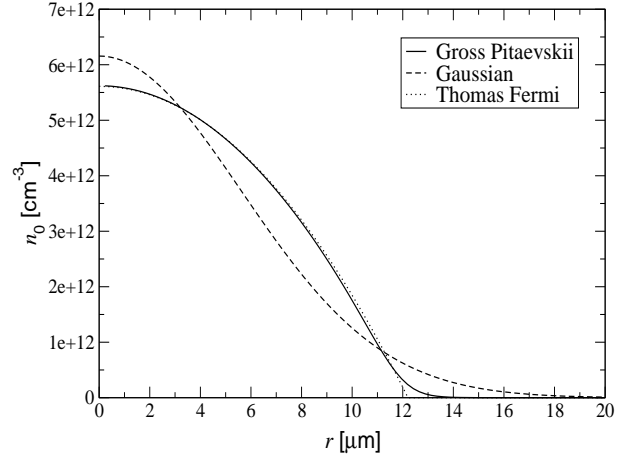


FIG. 10. The different initial states studied in a spherical harmonic trap with an oscillator length of about  $l_{\text{ho}} \cong 3 \mu\text{m}$ , i.e. a trap frequency of  $\omega_{\text{ho}} \cong 80 \text{ s}^{-1}$ , corresponding to the geometric mean of the frequencies used in the experiment [4] ( $\omega_{\text{ho}} = \sqrt[3]{\omega_{\text{radial}}^2 \omega_{\text{axial}}}$ ). The atoms are exposed to a magnetic field of  $B = 162.2 \text{ G}$  which implies a scattering length of about  $228 a_{\text{Bohr}}$ . Shown are the densities as functions of the radius corresponding to the exact ground state wave function given by the time independent Gross-Pitaevskii equation (solid line), and a Gaussian (dashed line), which is the best least square fit to the Thomas-Fermi approximation (dotted line). All densities correspond to a number of 17100 condensed atoms.

We have performed these studies similar to Subsection III C but in the presence of a trap. The trap has been idealized as a spherical harmonic oscillator potential  $V_{\text{trap}}(r) = \frac{1}{2}m\omega_{\text{ho}}^2 r^2$  with an oscillator frequency of about  $\omega_{\text{ho}} \cong 80 \text{ s}^{-1}$  and a resulting oscillator length of about  $l_{\text{ho}} \cong 3 \mu\text{m}$ . The trap parameters correspond to the geometric mean of the frequencies in Ref. [4], i.e.  $\omega_{\text{ho}} = \sqrt[3]{\omega_{\text{radial}}^2 \omega_{\text{axial}}}$ . We have studied initially pure condensates of  $N_0 = 17100$  atoms with different local densities. The different initial density profiles are shown in Fig. 10. The solid line is the density obtained from the exact solution to the time independent Gross-Pitaevskii equation for 17100 atoms with a scattering length of about  $a(162.2 \text{ G}) \cong 228 a_{\text{Bohr}}$ . This stationary condensate ground state exhibits a nearly perfect agreement with its Thomas Fermi approximation. The second state we have studied is a Gaussian (dashed line) which, for 17100 atoms, is the best least square fit to the Thomas-Fermi approximation (dotted line).



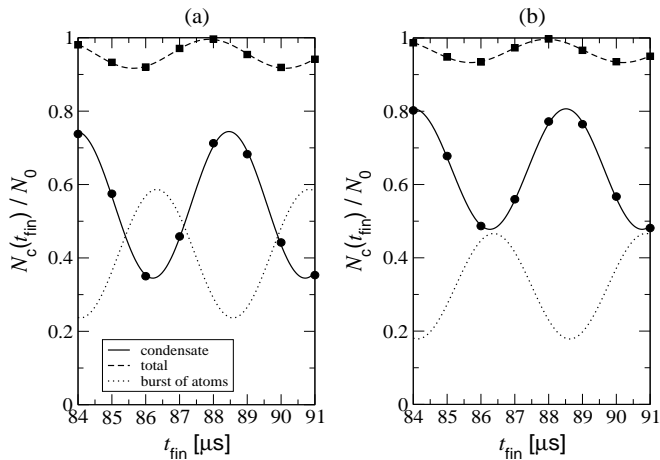


FIG. 11. The remaining fraction of condensate atoms,  $N_c(t_{\text{fin}})$ , (solid line), together with the molecular fraction (dashed line) and the burst of relatively hot unbound atoms (dotted line), as a function of the total time  $t_{\text{fin}}$  elapsed after the magnetic field pulse. The fractions are given relative to the initial number of atoms, i.e.  $N_0 = 17100$ . The calculations take into account the exact quantum dynamics of the trap for the initial state given, in Fig. 10, by the time independent Gross-Pitaevskii equation (a) and a Gaussian density distribution (b).

Figure 11 shows the condensate, molecular and burst fractions at the end of the pulse (Fig. 2) for the exact solution of the time independent Gross-Pitaevskii equation (a) and the Gaussian (b). The evolution times range between  $10 \mu\text{s}$  and  $17 \mu\text{s}$  such that the total time of the pulse ranges between  $84 \mu\text{s}$  and  $91 \mu\text{s}$ . The analysis of the trapped gas does not show any qualitative differences from its analogue in a homogeneous gas in Fig. 9. All components oscillate with the same frequency  $\nu_{\text{evolve}} = |E_{\text{b}}^{\text{evolve}}|/h$  and exhibit phase shifts similar to those in Fig. 9. Figure 11 reveals, however, that the relative magnitude of the components depends sensitively on the local densities in the initial inhomogeneous condensate.

To study the role of the trap potential and the one body kinetic energy we have performed the same analysis as in Fig. 11 in the local density approximation which accounts only for the dynamics of the nonlinear Schrödinger Eq. (3) for a uniform gas but with different densities, weighted according to the initial condensate wave function. The approximation, however, neglects the trapping potential and the one body kinetic energy. Figure 12 shows the different fractions of the gas under the same conditions as in Fig. 11. A comparison of Figs. 11 and 12 reveals no qualitative differences, but a quantitative dependence of all fractions of the gas on the trap potential and the one body kinetic energy. The oscillation frequencies are the same but the mean values and amplitudes vary. In the local density approximation the fraction of burst atoms results considerably smaller than in the exact calculation. A further analysis of the time

dependence of the condensate fraction, similar to Fig. 7, shows that the predominant influence of the trap potential occurs during the initial ramp to  $B = 155.5 \text{ G}$  in Fig. 2. In this period of the pulse sequence the scattering length becomes comparable to the oscillator length [14]. This additional length scale is neither accounted for in the homogeneous gas nor in the local density approximation. The results of this subsection show that a quantitative comparison of the magnitude of the different fractions in the gas with the experiment [4] should include the correct trap potential with the precise local densities in the initial condensate as well as the precise time dependence of the magnetic field pulse.

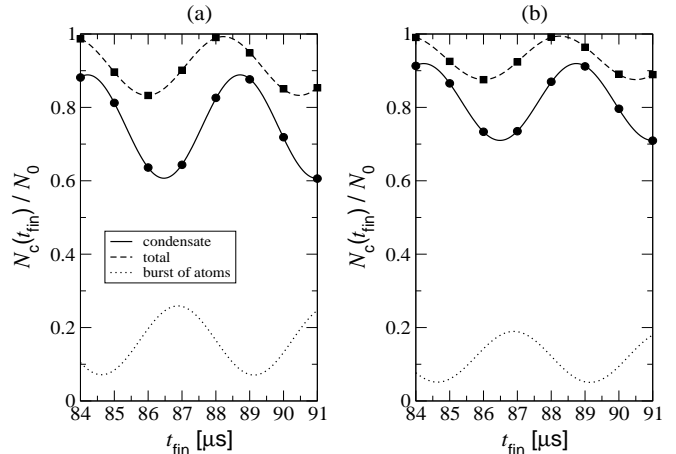


FIG. 12. The remaining fraction of condensate atoms,  $N_c(t_{\text{fin}})$ , (solid line), together with the molecular fraction (dashed line) and burst of relatively hot unbound atoms (dotted line), as a function of the total time  $t_{\text{fin}}$  elapsed after the magnetic field pulse. The fractions are given relative to the initial number of atoms, i.e.  $N_0 = 17100$ . The calculations are performed in the local density approximation for the initial state given, in Fig. 10, by the time independent Gross-Pitaevskii equation (a) and a Gaussian density distribution (b).

### E. Interpretation of the results

In the preceding sections we have analyzed the dynamics of an initially condensed Bose gas of  $^{85}\text{Rb}$  atoms exposed to a magnetic field pulse of the form in Fig. 2. We have identified the different fractions of unbound atoms in the gas as a remnant condensate and a burst of comparatively hot atoms with kinetic energies of about  $E_{1\text{B}}/k_{\text{B}} \gtrsim 100 \text{ nK}$ . We have further analyzed the dependence of the relevant physical observables on the precise external conditions. Our results strongly indicate that the fraction of missing atoms reported in [4] corresponds to atoms bound to dimer molecules that could not be detected.

Donley et al. [4] raised the question whether these molecules form a condensate. The analysis in Section

II provides a definite answer on the basis of the microscopic approach to the many body quantum dynamics: In Subsection IID we have predicted that the molecular fraction would stay confined in the atomic condensate in a ballistic expansion immediately after the pulse while the burst fraction of unbound pairs of atoms rapidly disperses. The expansion served as the first experimental technique to prove the presence of a condensate.

The formation of a molecular condensate can be physically understood from the nature of the external perturbation of the initial atomic condensate: The magnetic field pulse provides energy to form dimer molecules and correlated pairs of burst atoms but no momentum to drive their centers of mass. A further analysis of Eqs. (5), (16) and (20) shows that, indeed, the molecules as well as the correlated pairs of burst atoms exhibit the same momentum spread in their centers of mass as the condensate atoms. Momentum is transferred only to the relative coordinate of the burst atoms such that the total momentum of the pairs remains negligibly small. A typical density of a molecular condensate in a spherical trap is shown in Fig. 13.

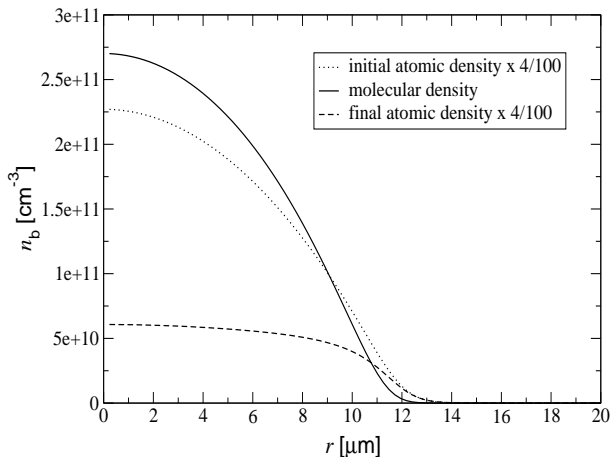


FIG. 13. The initial (dotted line) and final (dashed line) atomic condensate density, together with the molecular condensate density,  $n_b$ , (solid line) for  $t_{\text{evolve}} = 16 \mu\text{s}$  in a spherical trap. The curves correspond to the calculations in Fig. 11 (a). The atomic densities are multiplied by a factor of 0.04.

As a great advantage of the microscopic dynamics approach, the molecular condensate wave function,  $\Psi_b$  in Eq. (16), has been derived from the exact hierarchy of dynamic equations for correlation functions of field operators with the general Hamiltonian Eq. (1) using a systematic truncation scheme. Hence, the determination of the molecular condensate fraction does not rely upon any assumption on the existence of a molecular order parameter. The analysis in this subsection is independent of the precise trap geometry or the density profile of the initial state.

## ACKNOWLEDGMENTS

We would like to thank Eite Tiesinga, Eric Bolda, Paul Julienne, and Bill Phillips for very inspiring and helpful discussions. This work has been supported by the Alexander von Humboldt-Foundation (T.K., T.G.), the European Community under contract no. HPMF-CT-1999-0023 (T.G.), and the United Kingdom EPSRC.

## APPENDIX A: THE MICROSCOPIC QUANTUM DYNAMICS APPROACH

In this appendix we will derive the first order microscopic dynamics approach to Bose condensed gases. The present derivation includes the explicit dynamics of the non-condensed fraction which is not considered in Ref. [5].

### 1. Dynamic equations for cumulants

In general, the quantum state of a gas at time  $t$  is described by a statistical operator  $\rho(t)$  and the corresponding expectation value of an operator  $\mathcal{O}$  reads:

$$\langle \mathcal{O} \rangle_t = \text{Tr} [\rho(t)\mathcal{O}]. \quad (\text{A1})$$

Quantum expectation values of normal ordered products of field operators are termed correlation functions. The exact dynamics of the infinite hierarchy of correlation functions is given by

$$i\hbar \frac{\partial}{\partial t} \langle \psi^\dagger(\mathbf{x}_n) \cdots \psi(\mathbf{x}_1) \rangle_t = \langle [\psi^\dagger(\mathbf{x}_n) \cdots \psi(\mathbf{x}_1), H] \rangle_t, \quad (\text{A2})$$

where  $n$  denotes the number of field operators in the normal ordered product and  $H$  is the quite general Hamiltonian in Eq. (1). The set of Eqs. (A2) is equivalent to the many body Schrödinger equation and determines all physical properties of a gas of atoms. Due to the interaction term in Eq. (1) any finite subsystem of Eqs. (A2) does not close, and any attempt of an approximate solution relies upon a consistent way of truncation. A systematic truncation scheme, based on cumulants of correlation functions, has been proposed in [10] for the dynamics of fermionic many body systems on short time scales. The extension of this work to interacting Bose gases [5], with a modified truncation scheme, allows to describe the dynamics on the time scales that are relevant in this article.

The cumulants considered here are equivalent to the connected  $n$ -point functions and are usually defined as derivatives of a generating functional (cf., e.g., [15]):

$$\langle \psi^\dagger(\mathbf{x}_n) \cdots \psi(\mathbf{x}_1) \rangle^c = \frac{\delta}{\delta J(\mathbf{x}_n)} \cdots \frac{\delta}{\delta J^*(\mathbf{x}_1)} \times \ln \left\langle e^{\int d^3x [J^*(\mathbf{x})\psi(\mathbf{x}) + J(\mathbf{x})\psi^\dagger(\mathbf{x})]} \right\rangle_{J=J^*=0}. \quad (\text{A3})$$

The cumulants may also be derived recursively, and the first three orders read:

$$\begin{aligned}
\langle \mathcal{O}_1 \rangle &= \langle \mathcal{O}_1 \rangle^c, \\
\langle \mathcal{O}_1 \mathcal{O}_2 \rangle &= \langle \mathcal{O}_1 \mathcal{O}_2 \rangle^c + \langle \mathcal{O}_1 \rangle^c \langle \mathcal{O}_2 \rangle^c, \\
\langle \mathcal{O}_1 \mathcal{O}_2 \mathcal{O}_3 \rangle &= \langle \mathcal{O}_1 \mathcal{O}_2 \mathcal{O}_3 \rangle^c + \langle \mathcal{O}_1 \rangle^c \langle \mathcal{O}_2 \rangle^c \langle \mathcal{O}_3 \rangle^c \\
&\quad + \langle \mathcal{O}_1 \rangle^c \langle \mathcal{O}_2 \mathcal{O}_3 \rangle^c + \langle \mathcal{O}_2 \rangle^c \langle \mathcal{O}_1 \mathcal{O}_3 \rangle^c \\
&\quad + \langle \mathcal{O}_3 \rangle^c \langle \mathcal{O}_1 \mathcal{O}_2 \rangle^c, \\
&\vdots
\end{aligned} \tag{A4}$$

For an ideal Bose gas, in the grand canonical thermal equilibrium, all cumulants containing more than two field operators vanish. This is a consequence of Wick's theorem in statistical mechanics according to which every number conserving normal ordered correlation function can be expressed as a sum of products of all possible pair contractions conserving the operator ordering. Moreover, as the expectation value of a single field vanishes, the second order cumulants become  $\langle \mathcal{O}_1 \mathcal{O}_2 \rangle = \langle \mathcal{O}_1 \mathcal{O}_2 \rangle^c$ . In accordance with Eq. (A4) the cumulants of an order higher than two vanish. In an interacting gas the higher order cumulants thus provide a measure for the deviation of the state of the gas from thermal equilibrium.

For the applications discussed in this article, with a condensate present in the gas, the relevant cumulants contain; the non number conserving condensate wave function  $\Psi(\mathbf{x}, t) = \langle \psi(\mathbf{x}) \rangle_t^c$ , the pair function  $\Phi(\mathbf{x}, \mathbf{y}, t) = \langle \psi(\mathbf{y}) \psi(\mathbf{x}) \rangle_t^c$  and the density matrix of the non condensed fraction  $\Gamma(\mathbf{x}, \mathbf{y}, t) = \langle \psi^\dagger(\mathbf{y}) \psi(\mathbf{x}) \rangle_t^c$ . The cumulant approach consists in transforming the exact hierarchy of dynamic Eqs. (A2) into an equivalent set of equations of motion for cumulants. The exact dynamic equations for the cumulants up to the second order are given explicitly in Ref. [5]. The truncation scheme of Ref. [5] consists in retaining, to the order of  $n$ , the exact dynamic equations for cumulants up to the order of  $n$  as well as the free time evolution of the cumulants of the order of  $n+1$  and  $n+2$ . The free time evolution of the cumulants of the order of  $n+1$  and  $n+2$  is obtained by neglecting, in their dynamic equations, all products of cumulants containing  $n+3$  and  $n+4$  field operators.

The first order microscopic dynamics approach ( $n=1$ ) results in a closed nonlinear Schrödinger equation for the mean field  $\Psi$  that allows us to describe the dynamics of a condensate close to but also far away from thermal equilibrium [5]. The first order dynamic equations that lead to the non-linear Schrödinger equation read [5]:

$$\begin{aligned}
i\hbar \frac{\partial}{\partial t} \Psi(\mathbf{x}, t) &= H_{1B}(\mathbf{x}) \Psi(\mathbf{x}, t) \\
&\quad + \int d^3y V(\mathbf{x} - \mathbf{y}, t) \Psi^*(\mathbf{y}, t) \\
&\quad \times \left[ \Phi(\mathbf{x}, \mathbf{y}, t) + \Psi(\mathbf{x}, t) \Psi(\mathbf{y}, t) \right],
\end{aligned} \tag{A5}$$

$$\begin{aligned}
i\hbar \frac{\partial}{\partial t} \Phi(\mathbf{x}_1, \mathbf{x}_2, t) &= H_{2B}(\mathbf{x}_1, \mathbf{x}_2) \Phi(\mathbf{x}_1, \mathbf{x}_2, t) \\
&\quad + V(\mathbf{x}_1 - \mathbf{x}_2, t) \Psi(\mathbf{x}_1, t) \Psi(\mathbf{x}_2, t).
\end{aligned} \tag{A6}$$

Here the one and two-body Hamiltonians are denoted by

$$\begin{aligned}
H_{1B}(\mathbf{x}) &= -\hbar^2 \nabla^2 / 2m + V_{\text{trap}}(\mathbf{x}), \\
H_{2B}(\mathbf{x}_1, \mathbf{x}_2) &= H_{1B}(\mathbf{x}_1) + H_{1B}(\mathbf{x}_2) + V(\mathbf{x}_1 - \mathbf{x}_2, t).
\end{aligned} \tag{A7}$$

Equations (A5) and (A6) include the loss of condensate atoms into the non-condensed fraction as well as the back action of non condensed atoms on the condensate on time scales comparable to collisional durations. On longer time scales the non condensed fraction becomes dilute and its back action is neglected.

The first order dynamics of the non-condensed fraction is determined through the conservation of the total number of atoms in the gas:

$$N = \int d^3x [\Gamma(\mathbf{x}, \mathbf{x}, t) + |\Psi(\mathbf{x}, t)|^2] \tag{A8}$$

is a constant of motion. The corresponding approximate dynamic equation for  $\Gamma$  is then obtained from its exact counterpart in Ref. [5] through

$$\begin{aligned}
i\hbar \frac{\partial}{\partial t} \Gamma(\mathbf{x}_1, \mathbf{x}_2, t) &= \left\{ H_{1B}(\mathbf{x}_1) \Gamma(\mathbf{x}_1, \mathbf{x}_2, t) \right. \\
&\quad + \int d^3y V(\mathbf{x}_1 - \mathbf{y}, t) \Phi^*(\mathbf{y}, \mathbf{x}_2, t) \\
&\quad \times \left[ \Phi(\mathbf{x}_1, \mathbf{y}, t) + \Psi(\mathbf{x}_1, t) \Psi(\mathbf{y}, t) \right] \left. \right\} \\
&\quad - \{\mathbf{x}_1 \leftrightarrow \mathbf{x}_2\}^*.
\end{aligned} \tag{A9}$$

The density matrix of the non-condensed fraction  $\Gamma(\mathbf{x}_1, \mathbf{x}_2, t)$ , as given in Eq. (A9), is determined solely by the evolution of  $\Psi$  from the initial time  $t_0$  up to the present time  $t$ .

## 2. First order dynamics

In this subsection we will derive the non-linear Schrödinger Eq. (3) as well as Eqs. (5) and (6) for the pair function and the density matrix of the non-condensed fraction, respectively. For the purpose of solving Eqs. (A6) and (A9) formally in terms of the mean field  $\Psi$  it is convenient to change the representation from the configuration space to the one body energy states of the trap potential  $|\phi_i\rangle$  or, for a homogeneous gas, into Fourier space. The corresponding single mode annihilation and creation operators obey the commutation relations  $[a_i, a_j^\dagger] = \delta_{ij}$  and the field operator becomes  $\psi(\mathbf{x}) = \sum_i \phi_i(\mathbf{x}) a_i$ . In this new representation the cumulants up to the second order read:  $\Psi_i(t) = \langle a_i \rangle_t^c$ ,  $\Phi_{ij}(t) = \langle a_j a_i \rangle_t^c$ , and  $\Gamma_{ij}(t) = \langle a_j^\dagger a_i \rangle_t^c$ . We will abbreviate the trap states  $|\phi_i\rangle$  by  $|i\rangle$  in the following.

In the new representation Eq. (A6) for the pair function assumes the form

$$\begin{aligned}
i\hbar \frac{\partial}{\partial t} \Phi_{ij}(t) &= (E_i + E_j) \Phi_{ij}(t) \\
&+ \sum_{k_1, k_2} \langle i, j | V(t) | k_1, k_2 \rangle [\Phi_{k_1 k_2}(t) + \Psi_{k_1}(t) \Psi_{k_2}(t)],
\end{aligned} \tag{A10}$$

where  $E_i$  is the eigenvalue of  $H_{1B}$  with respect to the mode function  $\phi_i(\mathbf{x})$ . Equation (A10) can be solved formally in terms of the two body Green's function [16]:

$$\begin{aligned}
\Phi_{ij}(t) &= \sum_{k_1, k_2} \left[ \langle i, j | U_{\text{trap}}^{2B}(t, t_0) | k_1, k_2 \rangle \Phi_{k_1 k_2}(t_0) \right. \\
&\left. + \int_{t_0}^t d\tau \langle i, j | G_{2B}^{(+)}(t, \tau) V(\tau) | k_1, k_2 \rangle \Psi_{k_1}(\tau) \Psi_{k_2}(\tau) \right].
\end{aligned} \tag{A11}$$

Here  $G_{2B}^{(+)}$  is the retarded two-body Green's function,

$$\left( i\hbar \frac{\partial}{\partial t} - H_{2B}(t) \right) G_{2B}^{(+)}(t, \tau) = \delta(t - \tau), \tag{A12}$$

which vanishes for  $t < \tau$ . The retarded Green's function is related to the time development operator of two trapped interacting atoms, given by the time ordered exponential

$$U_{\text{trap}}^{2B}(t, \tau) = \mathcal{T} \exp \left[ -\frac{i}{\hbar} \int_{\tau}^t dt' H_{2B}(t') \right], \tag{A13}$$

through

$$G_{2B}^{(+)}(t, \tau) = \frac{1}{i\hbar} \theta(t - \tau) U_{\text{trap}}^{2B}(t, \tau), \tag{A14}$$

where  $\theta(t - \tau)$  is the step function that yields unity for  $t > \tau$  and vanishes elsewhere. In all applications in this article the gas is a dilute condensate at the initial time  $t_0$ . The initial pair function  $\Phi_{k_1 k_2}(t_0)$  on the right hand side of Eq. (A11) can then be neglected [5] and Eq. (A11) thus yields Eq. (5) in position space.

Inserting Eq. (A11) into Eq. (A5) for the mean field leads to the closed non-linear Schrödinger equation

$$\begin{aligned}
i\hbar \frac{\partial}{\partial t} \Psi_i(t) &= E_i \Psi_i(t) \\
&+ \sum_{k_1, k_2, k_3} \int_{t_0}^{\infty} d\tau \langle i, k_3 | T_{2B}^{(+)}(t, \tau) | k_1, k_2 \rangle \\
&\quad \times \Psi_{k_1}(\tau) \Psi_{k_2}(\tau) \Psi_{k_3}^*(t),
\end{aligned} \tag{A15}$$

where  $T_{2B}^{(+)}$  denotes the retarded two-body transition matrix in the time domain:

$$T_{2B}^{(+)}(t, \tau) = V(t) \delta(t - \tau) + V(t) G_{2B}^{(+)}(t, \tau) V(\tau). \tag{A16}$$

As in all applications in this article the trap potential is slowly varying on the spatial scale determined by the range of the binary interaction  $V(t)$  the thermodynamic

limit in the relative motion of two atoms can be performed in the collision term in Eq. (A15) [5]. The coupling function in Eq. (4) thus involves the time development operator of the relative motion of two atoms in free space, denoted by  $U_{2B}(t, \tau)$ . Transformed back to the position space Eq. (A15) then yields the nonlinear Schrödinger Eq. (3).

In the first order microscopic dynamics approach the pair function, as given by Eq. (A11) with  $\Phi_{k_1 k_2}(t_0) = 0$ , determines the density matrix of the non condensed fraction: Differentiation with respect to the time  $t$  shows that

$$\Gamma_{ij}(t) = \sum_k \Phi_{ik}(t) \Phi_{jk}^*(t) \tag{A17}$$

is the solution of Eq. (A9) for an initial pure condensate, i.e.  $\Gamma_{ij}(t_0) = 0$ , which derives Eq. (6). The density matrix of the non-condensed fraction thus assumes the form of a partial trace over one coordinate of a two body pure state. The corresponding occupation numbers, i.e. the diagonal elements

$$\Gamma_{ii}(t) = \sum_k |\Phi_{ik}(t)|^2, \tag{A18}$$

are positive, independent of the specific choice of the basis set.

As shown in Subsections IIC and IID the non-condensed fraction consists of a molecular part and a burst of atoms emitted in pairs from the condensate with a comparatively fast relative motion. This separation corresponds to a ballistic expansion of a gas that is released from a trap. The density of molecules in the bound state  $\phi_b$  is described by the mean field  $\Psi_b$  in Eq. (16). In analogy to the collision term of the nonlinear Schrödinger Eq. (A15) the molecular mean field can be expressed in terms of the atomic condensate wave function  $\Psi$ :

$$\Psi_b(\mathbf{R}, t) = -\frac{1}{\sqrt{2}} \int_{t_0}^{\infty} d\tau \Psi^2(\mathbf{R}, \tau) \frac{\partial}{\partial \tau} h_b(t, \tau). \tag{A19}$$

The corresponding coupling function,  $h_b(t, \tau)$ , involves the overlap of the molecular bound state wave function  $\phi_b$  and the two body time development operator which, in all applications in this article, is excellently approximated by the thermodynamic limit:

$$h_b(t, \tau) = (2\pi\hbar)^{3/2} \langle \phi_b | U_{2B}(t, \tau) | 0 \rangle \theta(t - \tau). \tag{A20}$$

The energy spectrum of the burst atoms in Eq. (21) involves an amplitude  $\Psi_{\mathbf{p}}(\mathbf{R})$ , similar to Eq. (A19), except that the bound state  $\phi_b$  is replaced by the stationary scattering state  $\phi_{\mathbf{p}}^{(+)}$  which is associated with the relative momentum  $\mathbf{p}$ , i.e.

$$\begin{aligned}
\Psi_{\mathbf{p}}(\mathbf{R}) &= -\frac{1}{\sqrt{2}} \int_{t_0}^{t_{\text{fin}}} d\tau \int d^3 R' d^3 r' \\
&\quad \times \Psi(\mathbf{R}' + \mathbf{r}'/2, \tau) \Psi(\mathbf{R}' - \mathbf{r}'/2, \tau) \\
&\quad \times \frac{\partial}{\partial \tau} \langle \mathbf{R}, \phi_{\mathbf{p}}^{(+)} | U_{\text{trap}}^{2B}(t_{\text{fin}}, \tau) | \mathbf{R}', \mathbf{r}' \rangle.
\end{aligned} \tag{A21}$$

Here,  $t_{\text{fin}}$  is the final time immediately after the pulse in Fig. 2. As  $\phi_{\mathbf{p}}^{(+)}(\mathbf{r})$  is not confined in space (see Appendix B) the coupling function corresponding to  $\Psi_{\mathbf{p}}(\mathbf{R})$  should explicitly account for the discrete nature of the trap states also in the relative motion of two atoms. In Section III we have determined the energy spectrum of the burst atoms for a homogeneous gas, i.e. in the absence of a trap potential. The coupling function of  $\Psi_{\mathbf{p}}$  then becomes similar to  $h_{\text{b}}(t, \tau)$  in Eq. (A20).

## APPENDIX B: TWO-BODY DYNAMICS

In Appendix A we have formulated the many body dynamics of a condensed gas in terms of the unitary time evolution operator of two atoms interacting through their inter-atomic potential. In this appendix we provide a practical approach to determine the relevant low energy time evolution of two  $^{85}\text{Rb}$  atoms that serves as an input to the microscopic dynamic description of a partially condensed gas exposed to the time dependent magnetic field discussed in Section III. The approach takes advantage of the fact that in all applications in this article the binary interaction of  $^{85}\text{Rb}$  is dominated by the presence of a shallow  $s$  wave bound state.

### 1. Resonance enhanced scattering

In ultra-cold dilute gases the energies of two colliding atoms are usually sufficiently small for the differential cross sections to become isotropic. In accordance with effective range theory [16] the  $s$  wave scattering amplitude can then be expanded as

$$f_0(k) = -a + ia(ka) + \mathcal{O}(k^2) = \frac{-a}{1 + ika} + \mathcal{O}(k^2), \quad (\text{B1})$$

where  $k$  is the wave number that is related to the relative momentum of two colliding atoms through  $p = \hbar k$ . Equation (B1) effectively provides an expansion in terms of  $kl$ , where the first dominant length scale  $l$  is given by the  $s$  wave scattering length  $a$ . The next correction term involves the effective range of the binary potential  $V$  [16], denoted as  $r_{\text{eff}}$  in the following. In general, both  $a$  and  $r_{\text{eff}}$  depend sensitively on the detailed shape of  $V$ .

When the binary potential supports a shallow  $s$  wave bound state the scattering length is positive and may by far exceed all the other length scales set by  $V$ . This situation is sometimes referred to as a zero energy resonance [16]. The scattering amplitude is then given by  $-a/(1 + ika)$ , as obtained from the right hand side of Eq. (B1), which corresponds to the contact potential [17]. Extending the collision energies  $p^2/m$  into the complex plane Eq. (B1) yields the  $T$  matrix [16] of the contact potential which assumes the separable, i.e. factorized, form:

$$T_{2\text{B}}(z) = \frac{|\chi\rangle\xi\langle\chi|}{1 + i\sqrt{mz/\hbar^2}a}, \quad (\text{B2})$$

where  $z = p^2/m + i\varepsilon$  is a complex energy variable and the complex square root is chosen with a positive imaginary part. The wave function  $|\chi\rangle$  and the amplitude  $\xi$  are obtained as  $\langle\mathbf{r}|\chi\rangle = \delta(\mathbf{r})$  and  $\xi = 4\pi\hbar^2 a/m$ , respectively. The  $T$  matrix determines all eigenstates of the two body Hamiltonian. The pole on the right hand side of Eq. (B2) indicates that the contact potential with a positive scattering length supports a single  $s$  wave bound state with the binding energy

$$E_{\text{b}} = -\hbar^2/ma^2. \quad (\text{B3})$$

The separable form of Eq. (B2) is quite general whenever the  $T$  matrix is dominated by the pole of a shallow  $s$  wave bound state  $\phi_{\text{b}}$ . A spectral decomposition of the two body Hamiltonian then implies that at low collision energies the  $T$  matrix is well approximated by [16]

$$T_{2\text{B}}(z) = \frac{|\chi\rangle\xi\langle\chi|}{1 - \xi\langle\chi|G_0(z)|\chi\rangle}, \quad (\text{B4})$$

where

$$\begin{aligned} |\chi\rangle &= V|\phi_{\text{b}}\rangle, \\ \xi &= 1/\langle\phi_{\text{b}}|V|\phi_{\text{b}}\rangle \end{aligned} \quad (\text{B5})$$

and  $G_0(z) = (z + \hbar^2\Delta/m)^{-1}$  is the free energy dependent Green's function of the relative motion of two atoms. In few body scattering theory Eq. (B5) is usually referred to as the unitary pole approximation [18]. A further analysis shows that the  $T$  matrix in Eq. (B4) has a pole at the exact bound state energy of the potential  $V$ . The wave function  $\chi(r)$  accounts for the spatial extent of  $V$ .

The long range behavior of inter-atomic potentials is determined by the van der Waals dispersion interaction  $V_{\text{vdW}}(r) = -C_6/r^6$ . The spatial extent of  $V$  is then characterized by the van der Waals length  $l_{\text{vdW}} = (mC_6/\hbar^2)^{1/4}$ . As shown by Gribakin and Flambaum [19] the next correction to the binding energy for an inter-atomic potential modifies Eq. (B3) to [20]:

$$E_{\text{b}} = -\hbar^2/m(a - \bar{a})^2. \quad (\text{B6})$$

Here  $\bar{a}$  is the mean scattering length given in terms of the  $\Gamma$  function through

$$\bar{a} = \frac{1}{2\sqrt{2}}l_{\text{vdW}}\frac{\Gamma(3/4)}{\Gamma(5/4)}. \quad (\text{B7})$$

Figure 14 illustrates the dependence of the bound state energy of the shallow  $s$  wave bound state of the  $^{85}\text{Rb}$  pair interaction on the magnetic field  $B$ . The binding energies obtained from Eq. (B6) are sufficiently accurate to match a recent exact coupled channels scattering calculation [21]. Although the  $^{85}\text{Rb}$  dimer, in the vicinity of the Feshbach resonance, is particularly weakly bound in comparison to usual molecular ground states Fig. 14 exhibits a pronounced difference between Eqs. (B3) and (B6). This deviation from the zero energy resonance situation is related to the large van der Waals length of about  $l_{\text{vdW}} = 164 a_{\text{Bohr}}$ .

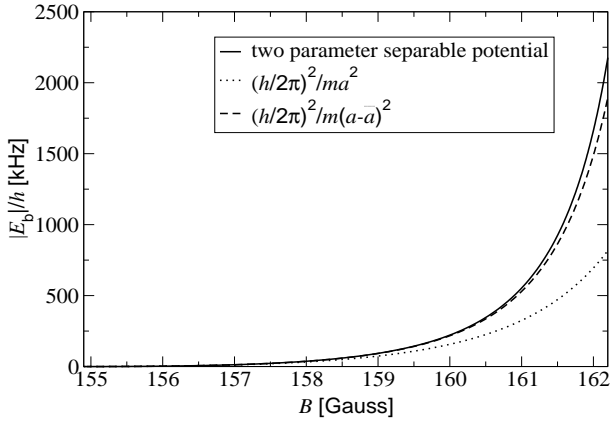


FIG. 14. The energy of the uppermost  $s$  wave bound state below threshold of two  $^{85}\text{Rb}$  atoms,  $E_b$ , as a function of the magnetic field strength  $B$ . The dotted line shows Eq. (B3) which corresponds to a zero energy resonance, with  $a(B)$  determined from Eq. (23), using  $B_0 = 154.9\text{ G}$ ,  $\Delta B = 11.0\text{ G}$ , and  $a_{\text{bg}} = -450 a_{\text{Bohr}}$ . The dashed line shows Eq. (B6) which accounts for the van der Waals interaction using  $C_6 = 4660$  a.u. [13]. The dashed curve can be compared directly with a recent exact coupled channels scattering calculation [21]. The solid line is obtained from the binding energies of two parameter separable potentials with the rounded parameter  $\eta = 5000 \times ma_{\text{Bohr}}^2/\hbar$  and the scattering length chosen in accordance with Eq. (23).

## 2. The separable potential approach

Direct insertion shows that Eq. (B4) exactly solves the Lippmann-Schwinger equation [16]

$$T_{2\text{B}}(z) = V + VG_0(z)T_{2\text{B}}(z) \quad (\text{B8})$$

as long as the actual potential  $V$  is replaced by the separable potential

$$V_{\text{sep}} = |\chi\rangle\xi\langle\chi|. \quad (\text{B9})$$

Since the pioneering work of Lovelace [22] separable expansions of potentials [23] have played an important role in nuclear few body physics, as they provide a systematic approach to solve two body scattering problems analytically in a limited range of collision energies. In this subsection we shall determine a separable potential of the form of Eq. (B9) that accurately describes the dynamics of two  $^{85}\text{Rb}$  atoms in the relevant range of magnetic fields and collision energies.

The unitary pole approximation in Eq. (B5) is obtained from spectral properties of the two body Hamiltonian and thus applies to inter-atomic potentials [24]. Equation (B5) reproduces the exact bound state energy of  $V$  but the scattering length is only approximate. A further improvement can be achieved by choosing  $|\chi\rangle$  and  $\xi$  in such a way that the separable potential in Eq. (B9) matches both the energy of the last  $s$  wave bound state and the scattering length of  $V$  at the actual magnetic

field. At the low collision momenta under consideration the corresponding plane wave states do not resolve the functional form of the wave function  $\chi(r)$ . The specific form of  $\chi(r)$  is thus not relevant as long as  $\chi(r)$  decays in space on the length scale set by the van der Waals length. We have chosen a Gaussian form which in momentum space is given by

$$\chi(p) = \langle \mathbf{p} | \chi \rangle = (2\pi\hbar)^{-3/2} e^{-\eta p^2/2m\hbar}. \quad (\text{B10})$$

In position space  $|\chi\rangle$  is of the form  $\chi(r) \propto \exp(-r^2/2\sigma^2)$  with a range parameter  $\sigma = \sqrt{\hbar\eta/m}$ . The separable potential is then parametrized by the two constants  $\xi$  and  $\eta$ . These parameters have to be determined at each magnetic field through matching the binding energy and scattering length of the separable potential to the values of  $E_b$  and  $a$  of the actual interaction  $V$ . The bound state energy of the separable potential is the real energy  $z = E_b$  at the pole of the  $T$  matrix in Eq. (B4), i.e.  $E_b$  is determined through

$$1 - \xi \langle \chi | G_0(E_b) | \chi \rangle = 0. \quad (\text{B11})$$

The scattering length is obtained from the zero energy limit of the  $T$  matrix as

$$\begin{aligned} a &= (2\pi\hbar)^3 \frac{m}{4\pi\hbar^2} \langle 0 | T_{2\text{B}}(0) | 0 \rangle \\ &= \frac{m}{4\pi\hbar^2} \frac{(2\pi\hbar)^3 |\langle 0 | \chi \rangle|^2}{1/\xi - \langle \chi | G_0(0) | \chi \rangle}. \end{aligned} \quad (\text{B12})$$

It turns out that the optimized parameter  $\eta$  is independent of  $B$  with the corresponding range parameter  $\sigma = \sqrt{\hbar\eta/m}$  roughly given by  $l_{\text{vdW}}/2$ . In the applications in this article we have used the rounded value of  $\eta = 5000 \times ma_{\text{Bohr}}^2/\hbar$  and determined  $\xi(B)$  in such a way that the separable potential matches exactly the dependence of the scattering length on the magnetic field in Eq. (23). The resulting dependence of the binding energy of the separable potential on the magnetic field  $B$  is shown in Fig. 14. The separable potential approach, as proposed in this subsection, does not depend upon the accuracy of model potentials for all scattering channels and, instead, describes the complete low energy collision dynamics in terms of the scattering length  $a$  and the van der Waals dispersion coefficient  $C_6$ . Both parameters of the actual binary potential are accessible to experiment [25,13].

To illustrate the degree of accuracy of the proposed approach we shall provide a comparison of the low energy scattering properties obtained from the separable potential with the exact solution of the Schrödinger equation for a well known inter-atomic interaction. We have chosen the scattering of two ground state  $^4\text{He}$  atoms for this comparison as the binary potential supports a single shallow  $s$  wave bound state and, within several decades of intensive study, all properties of the interaction have been determined very accurately, to a large extent, from first principle calculations [26]. The scattering length and

the binding energy have been determined recently from experiment in Ref. [27].

We have determined the separable potential, as given through Eqs. (B9) and (B10), that corresponds to the Tang, Toennies and Yiu (TTY)  ${}^4\text{He}$  interaction [26] with  $a = 188 a_{\text{Bohr}}$  and  $C_6 = 1.461$  a.u.. For  ${}^4\text{He}$  the ratio of the scattering length and the effective range,  $a/r_{\text{eff}}$  is of the order of magnitude of 14. Figure 15 shows the exact radial probability distribution of the bound state wave function  ${}^4\text{He}_2$  as well as the shallow  $s$  wave bound state of  ${}^{85}\text{Rb}$ , corresponding to the separable potential approach at a magnetic field of 162.2 G, as obtained from the integral form of the Schrödinger equation

$$|\phi_b\rangle = G_0(E_b)V|\phi_b\rangle. \quad (\text{B13})$$

The radius is given on a logarithmic scale. According to Eq. (B13) the asymptotic functional behavior of both bound state wave functions at far relative distances of the two atoms is determined solely through the free Green's function evaluated at the binding energy  $E_b$ . As their molecular states are very weakly bound both wave functions extend far outside the range of their pair interaction.

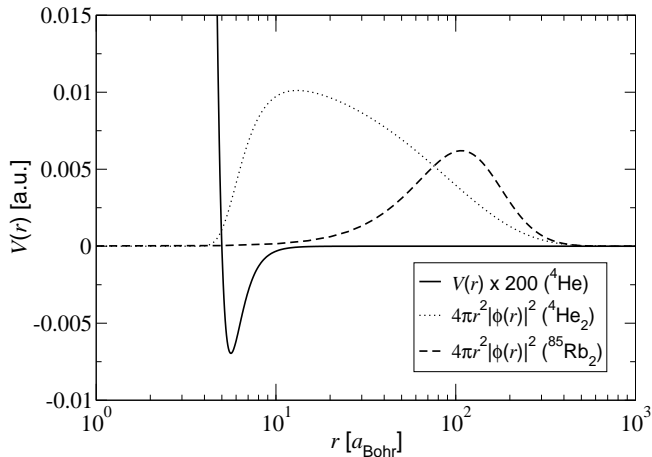


FIG. 15. The  ${}^4\text{He}$  binary (TTY) potential [26], and the radial probability densities corresponding to the shallow  $s$  wave bound states of  ${}^4\text{He}$  as well as  ${}^{85}\text{Rb}$ , as obtained from the separable potential, at a magnetic field strength of 162.2 G. The radius is given on a logarithmic scale.

For  ${}^4\text{He}$  the estimate corresponding to a zero energy resonance in Eq. (B3) gives  $|E_b|/h = 25486$  kHz while the formula of Gribakin and Flambaum in Eq. (B6) yields  $|E_b|/h = 26856$  kHz. The exact binding energy of the TTY potential is  $|E_b|/h = 27087$  kHz. The comparison shows that  $E_b$  and, in turn, the bound state wave function, are virtually completely determined by  $a$  and  $C_6$ . Figure 16 compares the exact wave function of  ${}^4\text{He}_2$  with the wave function obtained from the separable potential approach. The main small deviations occur in the region

of the inner well of the TTY potential in Fig. 15.

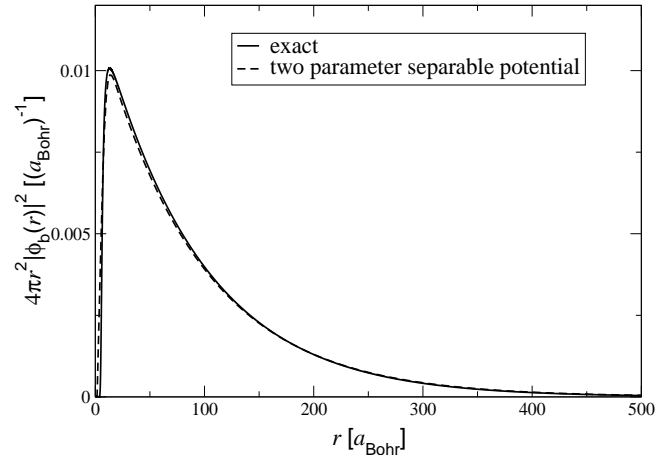


FIG. 16. The  ${}^4\text{He}$  radial probability density corresponding to the  $s$  wave bound state of  ${}^4\text{He}$  as obtained from the TTY potential [26] (solid line) and the separable potential approach (dashed line).

The  $T$  matrix determines the stationary scattering wave functions that correspond to the relative momentum  $\mathbf{p}$  through the Lippmann-Schwinger equation [16]

$$|\phi_{\mathbf{p}}^{(+)}\rangle = |\mathbf{p}\rangle + G_0(p^2/m + i0)T_{2B}(p^2/m + i0)|\mathbf{p}\rangle, \quad (\text{B14})$$

where the energy arguments “ $p^2/m + i0$ ” indicate that the real energy  $p^2/m$  is approached from the upper half of the complex plane. At low collision momenta  $p = \hbar k$  the stationary scattering states assume the asymptotic form

$$\phi_{\mathbf{p}}^{(+)}(\mathbf{r}) \sim \frac{1}{\sqrt{2\pi\hbar^3}} \left[ e^{i\mathbf{p}\cdot\mathbf{r}/\hbar} + f_0(k) \frac{e^{ipr/\hbar}}{r} \right], \quad (\text{B15})$$

as soon as the relative distance  $r$  exceeds by far the range of the potential. Figure 17 compares the  $s$  wave scattering amplitude in Eq. (B15), for two  ${}^{85}\text{Rb}$  atoms, obtained from the separable potential given by Eq. (B10), at  $B = 162.2$  G, with the amplitude of the contact potential in Eq. (B1).

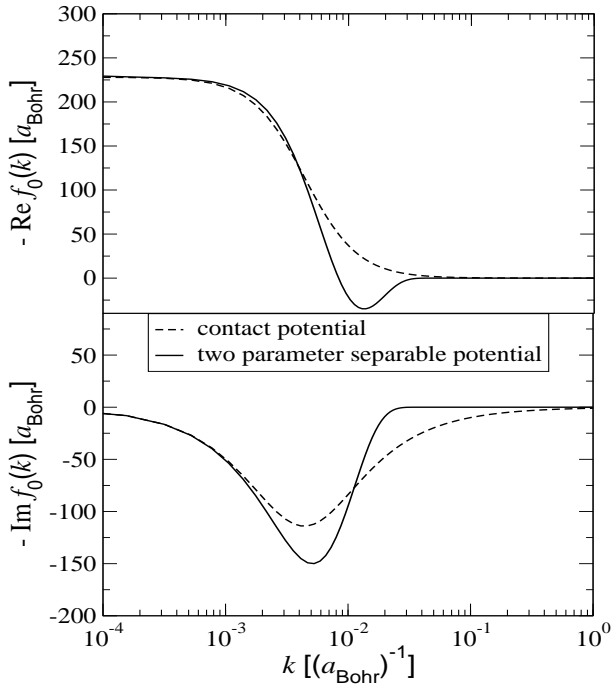


FIG. 17. The real and imaginary part of the  $s$ -wave scattering amplitude  $f_0(k)$  for  $^{85}\text{Rb}$ . The solid lines are obtained with the two parameter separable potential, the dashed lines in the contact potential approximation, both with a scattering length of  $a(162.2\text{ G}) = 228 a_{\text{Bohr}}$ . The wave number  $k$  is given on a logarithmic scale.

The pronounced deviations at  $k > 10^{-3} a_{\text{Bohr}}^{-1}$  are related to the large van der Waals length of the  $^{85}\text{Rb}$  interaction. This length scale is not accounted for by Eq. (B1). The  $s$  wave scattering amplitude approaches Eq. (B1) once the magnetic field is shifted further toward the Feshbach resonance at  $B = 154.9\text{ G}$ . The analogous comparison for  $^4\text{He}$  in Fig. 18 may illustrate to which degree of accuracy the scattering from the long range part of the binary interaction is described by the separable potential given by Eq. (B10). In accordance with the small van der Waals length of helium of about  $10 a_{\text{Bohr}}$  the deviations between the contact potential approach in Eq. (B1) and the exact scattering amplitude are much less pronounced. Even the small deviations, however, are correctly accounted for in the separable potential approach up to wave numbers of about  $3 \times 10^{-1} a_{\text{Bohr}}^{-1}$ . The length scale related to this upper limit of the wave numbers roughly corresponds to the radius of the inner well of the TTY potential in Fig. 15.

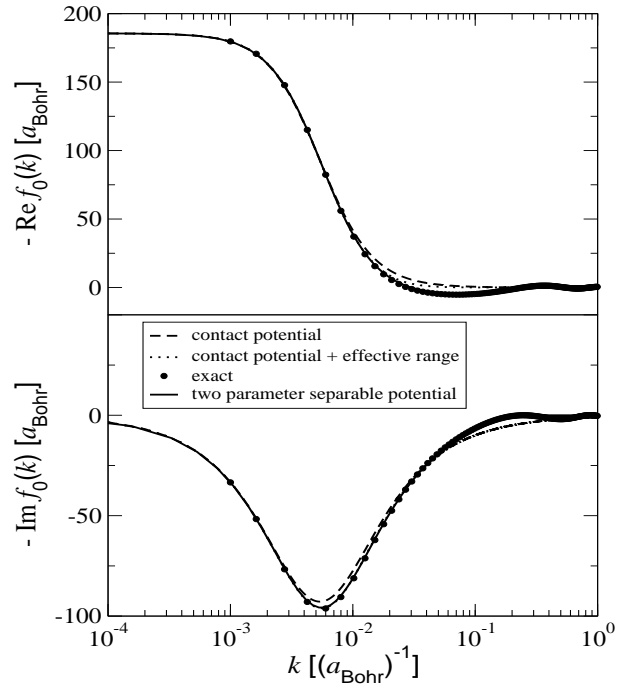


FIG. 18. The real and imaginary part of the  $s$ -wave scattering amplitude  $f_0(k)$  for  $^4\text{He}$ . The solid lines are obtained with the two parameter separable potential, the dashed lines in the contact potential approximation. The dotted lines show the scattering amplitude of an improved contact potential approach [28] that accounts for the effective range of the TTY potential. The bullets show the exact  $s$  wave scattering amplitude for the TTY potential [26].

### 3. Dynamics

In Subsection B2 we have analyzed the static low energy scattering properties of two  $^{85}\text{Rb}$  atoms at a given magnetic field. In this subsection we shall determine the collision dynamics that enters the many body theory of a partially condensed Bose gas through coupling functions of the form of Eq. (4). These coupling functions involve the complete unitary time evolution operator of two  $^{85}\text{Rb}$  atoms,  $U_{2\text{B}}(t, \tau)$ , exposed to a magnetic field pulse as shown in Fig. 2. We shall apply the separable potential approach of Subsection B2 to determine the coupling functions as the effective low energy potential renders the time dependent Schrödinger equation into a practical form.

We shall first determine the coupling function of the non-linear Schrödinger Eq. (3) denoted as  $h(t, \tau)$  in Eq. (4). The coupling function  $h(t, \tau)$  can be represented in terms of the time developed zero momentum plane wave of the relative motion of two atoms,  $|\zeta(t)\rangle = U_{2\text{B}}(t, \tau)|0\rangle$ , in the form:

$$h(t, \tau) = \theta(t - \tau)(2\pi\hbar)^3 \langle 0|V(t)|\zeta(t)\rangle. \quad (\text{B16})$$

The wave function  $|\zeta(t)\rangle$  is determined by the integral form of the time dependent Schrödinger equation through



$$|\zeta(t)\rangle = |0\rangle + \int_{\tau}^t d\tau' G_0(t-\tau')V(\tau')|\zeta(\tau')\rangle, \quad (\text{B17})$$

where  $G_0(t) = \theta(t)U_0(t)/i\hbar$  is the two body Green's function of the relative motion of two non-interacting atoms. To obtain the coupling function through Eq. (B16), on the basis of the actual binary potential  $V(t)$ , the Schrödinger Eq. (B17) needs to be solved for all times  $(t, \tau)$  between the initial and final time of the magnetic field pulse and, moreover, at all relative distances in the argument of the wave function  $\zeta(\mathbf{r}, t)$ .

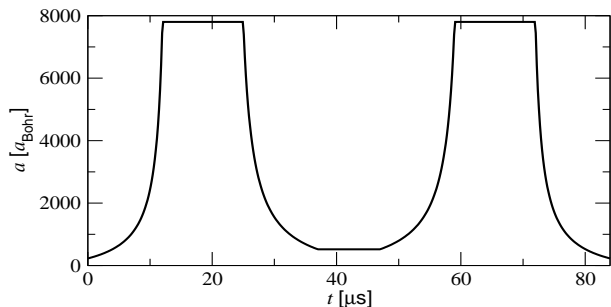


FIG. 19. The variation of the  $s$  wave scattering length  $a$  corresponding to the magnetic field pulse in Fig. 2.

The magnetic field pulse, however, releases a sufficiently small amount of energy to the gas that the actual potential  $V(t)$  in Eq. (B17) can be replaced by the effective low energy potential  $V_{\text{sep}}$  in Eq. (B9). Thereby, the amplitude  $\xi = \xi(t)$  accounts for the time dependence of the magnetic field through the variation of the scattering length  $a$  illustrated in Fig. 19. Equations (B16) and (B17) then yield the closed integral equation

$$h(t, \tau) = (2\pi\hbar)^3 |\langle 0 | \chi \rangle|^2 \xi(t, \tau) + \xi(t, \tau) \int_{\tau}^t d\tau' \langle \chi | G_0(t-\tau') | \chi \rangle h(\tau', \tau), \quad (\text{B18})$$

where  $\xi(t, \tau) \equiv \xi(t)\theta(t-\tau)$ . The separable form of the effective low energy potential leads to a closed dynamic equation for  $h(t, \tau)$  which avoids to explicitly take into account the spatial dependence of  $\zeta(\mathbf{r}, t)$ . The coupling function  $h(t, \tau)$ , as obtained from Eq. (B18), is shown in Figs. 4 and 6.

The coupling function associated with the molecular condensate wave function  $\Psi_b$  is given in Appendix A by Eq. (A20) and denoted as  $h_b(t, \tau)$ . In Section III  $|\Psi_b|^2$  describes the density of  $^{85}\text{Rb}_2$  molecules at time  $t_{\text{fin}}$ , immediately after the magnetic field pulse, in the bound state corresponding to the wave function in Fig. 15. The wave function  $\zeta(\mathbf{r}, t_{\text{fin}})$  in Eq. (B17) determines  $h_b(t_{\text{fin}}, \tau)$  through:

$$h_b(t_{\text{fin}}, \tau) = \theta(t_{\text{fin}} - \tau)(2\pi\hbar)^{3/2} \langle \phi_b | \zeta(t_{\text{fin}}) \rangle. \quad (\text{B19})$$

Taking advantage of the separable form of the effective low energy potential the Schrödinger Eq. (B17) in-

serted into Eq. (B19) determines  $h_b(t_{\text{fin}}, \tau)$  in terms of the known coupling function  $h(t, \tau)$ :

$$h_b(t_{\text{fin}}, \tau) = \theta(t_{\text{fin}} - \tau) \left[ (2\pi\hbar)^{3/2} \langle \phi_b | 0 \rangle + \int_{\tau}^{t_{\text{fin}}} dt \frac{\langle \phi_b | G_0(t_{\text{fin}} - t) | \chi \rangle}{\langle 0 | \chi \rangle} h(t, \tau) \right]. \quad (\text{B20})$$

The molecular coupling function  $h_b(t_{\text{fin}}, \tau)$ , as a function of  $\tau$ , is shown in Fig. 20 for the magnetic field pulse in Fig. 2. The calculation of  $h_b(t_{\text{fin}}, \tau)$  has been performed with the  $^{85}\text{Rb}_2$  wave function in Fig. 15 that corresponds to the shallow  $s$  wave bound state at the magnetic field of  $B = 162.2$  G at the end of the pulse sequence.

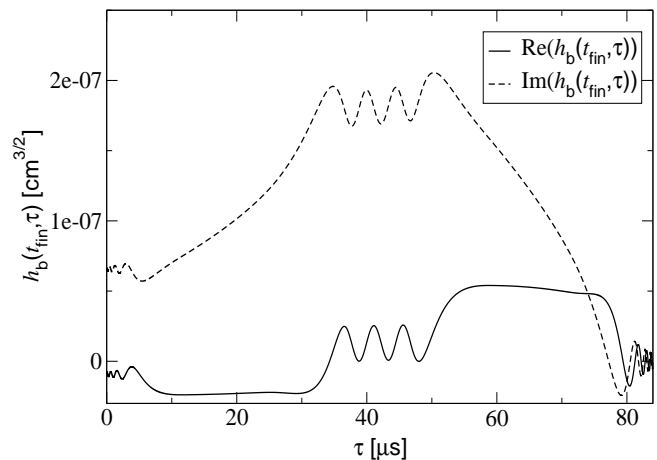


FIG. 20. The molecular coupling function  $h_b(t_{\text{fin}}, \tau)$ , as a function of  $\tau$ , corresponding to the molecular wave function of two  $^{85}\text{Rb}$  atoms at the final time of the pulse as depicted in Fig. 15. The magnetic field pulse corresponds to Fig. 2 with  $t_{\text{evolve}} = 10 \mu\text{s}$ .

A relation, similar to Eq. (B20), with  $\phi_b$  replaced by the stationary scattering state  $\phi_{\mathbf{p}}^{(+)}$  has been applied to calculate the spectral density of the pairs of burst atoms at a relative kinetic energy  $E_{\text{rel}} = p^2/m$  in a homogeneous gas in Subsection III C.

- 
- [1] J. Stenger, S. Inouye, M.R. Andrews, H.-J. Miesner, D.M. Stamper-Kurn, and W. Ketterle, Phys. Rev. Lett. **82**, 2422 (1999).
  - [2] R.H. Wynar, R.S. Freeland, D.J. Han, C. Ryu, and D.J. Heinzen, Science **287**, 1016 (2000).
  - [3] N.R. Claussen, E.A. Donley, S.T. Thompson, and C.E. Wieman, Phys. Rev. Lett. **89**, 010401 (2002).
  - [4] E.A. Donley, N.R. Claussen, S.T. Thompson, and C.E. Wieman, Nature (London) **417**, 529 (2002).

- [5] T. Köhler and K. Burnett, *Phys. Rev. A* **65**, 33601 (2002).
- [6] F. Dalfovo, S. Giorgini, L.P. Pitaevskii, and S. Stringari, *Rev. Mod. Phys.* **71**, 463 (1999).
- [7] S.J.J.M.F. Kokkelmans and M.J. Holland, LANL e-print cond-mat/0204504.
- [8] M. Mackie, K.-A. Suominen, and J. Javanainen, LANL e-print cond-mat/0205535.
- [9] E. Timmermans, P. Tommasini, R. Côté, M. Hussein, and A. Kerman, *Phys. Rev. Lett.* **83**, 2691 (1999).
- [10] J. Fricke, *Ann. Phys. (N.Y.)* **252**, 479 (1996).
- [11] A. Messiah, *Mécanique Quantique*, Tome 2 (Dunod, Paris, 1964).
- [12] W.C. Stwalley, *Phys. Rev. Lett.* **37**, 1628 (1976); E. Tiesinga, A.J. Moerdijk, B.J. Verhaar, and H.T.C. Stoof, *Phys. Rev. A* **46**, R1167 (1992); E. Tiesinga, B.J. Verhaar, and H.T.C. Stoof, *Phys. Rev. A* **47**, 4114 (1993); F.H. Mies, E. Tiesinga, and P.S. Julienne, *Phys. Rev. A* **61**, 022721 (2000).
- [13] J.L. Roberts, J.P. Burke Jr., N.R. Claussen, S.L. Cornish, E.A. Donley, and C.E. Wieman, *Phys. Rev. A* **64**, 024702 (2001).
- [14] The highest ratio of  $a/l_{ho}$  considered in the present applications is of the order of 15 %. If the magnetic field approached the Feshbach resonance even further the low energy binary scattering in the presence of the trap might no longer be well characterized by a scattering length [see E. Tiesinga, C.J. Williams, F.H. Mies, and P.S. Julienne, *Phys. Rev. A* **61**, 063416 (2000)].
- [15] S. Weinberg, *The Quantum Theory of Fields*, Volume 2 (Cambridge University Press, Cambridge, England, 1996).
- [16] R.G. Newton, *Scattering Theory of Waves and Particles* (Springer, New York, 1982).
- [17] J. Dalibard in *Proceedings of the International School of Physics Enrico Fermi CXL*, edited by M. Inguscio, S. Stringari and C.E. Wieman (IOS, Amsterdam, 1999).
- [18] W. Glöckle, *The Quantum Mechanical Few-Body Problem*, edited by W. Beiglböck (Springer, Berlin, 1983).
- [19] G.F. Gribakin and V.V. Flambaum, *Phys. Rev. A* **48**, 546 (1993).
- [20] We thank Paul Julienne for pointing this out to us.
- [21] The dependence of the binding energy on the magnetic field as obtained from the coupled channels calculation by S.J.J.M.F. Kokkelmans is given, e.g., in Fig. 5 of [4].
- [22] C. Lovelace, *Phys. Rev.* **135**, B1225 (1964).
- [23] V.B. Beliaev, *Lectures on the Theory of Few-body systems*, edited by K. Gaillard (Springer, Berlin, 1990).
- [24] The unitary pole approximation has been applied to inter-atomic potentials, e.g., to determine the bound states of the helium trimer molecule in G.C. Hegerfeldt and T. Köhler, *Phys. Rev. Lett.* **84**, 3215 (2000).
- [25] J.L. Roberts, N.R. Claussen, J.P. Burke Jr., C.H. Greene, E.A. Cornell, and C.E. Wieman, *Phys. Rev. Lett.* **81**, 5109 (1998).
- [26] K.T. Tang, J.P. Toennies, and C.L. Yiu, *Phys. Rev. Lett.* **74**, 1546 (1995).
- [27] R.E. Grisenti, W. Schöllkopf, J.P. Toennies, G.C. Hegerfeldt, T. Köhler, and M. Stoll, *Phys. Rev. Lett.* **85**, 2284 (2000).
- [28] E. Braaten, H.W. Hammer, and S. Hermans, *Phys. Rev. A* **63**, 063609 (2001).